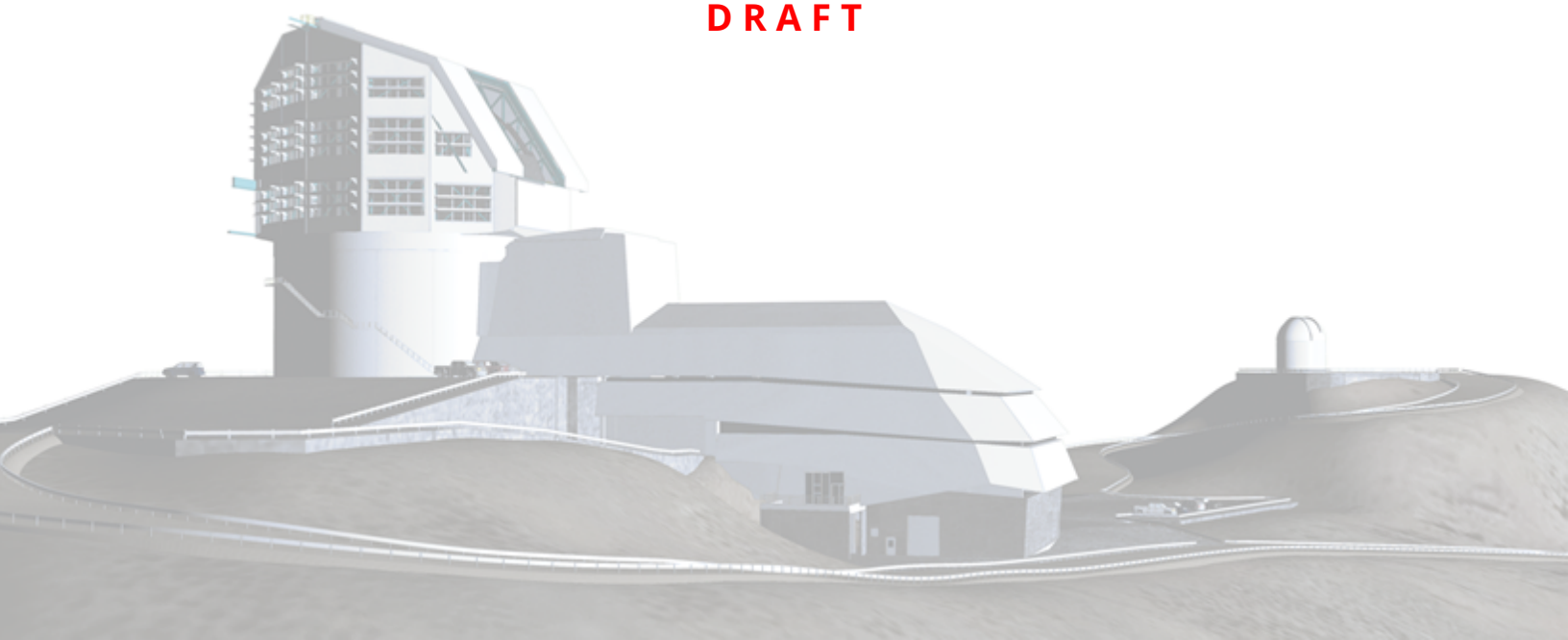

Vera C. Rubin Observatory
Systems Engineering

An Interim Report on the ComCam On-Sky Campaign

Many authors

SITCOMTN-149

Latest Revision: 2024-12-04

DRAFT

Abstract

A summary of what we have learned from the initial period of ComCam observing

Change Record

Version	Date	Description	Owner name
1	YYYY-MM-DD	Unreleased.	Robert Lupton

Document source location: `https://github.com/lsst-sitcom/sitcomtn-149`

Contents

An Interim Report on the ComCam On-Sky Campaign

1 Introduction

The Vera C. Rubin Observatory on-sky commissioning campaign using the Commissioning Camera (ComCam) began on 24 October 2024 and is forecasted to continue through mid-December 2024. This interim report provides a concise summary of our understanding of the integrated system performance based tests and analyses conducted during the first weeks of the ComCam on-sky campaign. The emphasis is distilling and communicating what we have learned about the system. The report is organized into sections to describe major activities during the campaign, as well as multiple aspects of the demonstrated system and science performance.

Warning: Preliminary Results

All of the results presented here are to be understood as work in progress using engineering data. It is expected at this stage, in the middle of on-sky commissioning, that much of the discussion will concern open questions, issues, and anomalies that are actively being worked by the team. Additional documentation will be provided as our understanding of the demonstrated performance of the as-built system progresses.

1.1 Charge

We identify the following high-level goals for the interim report:

- **Rehearse workflows for collaboratively developing documentation** to describe our current understanding of the integrated system performance, e.g., to support the development of planned Construction Papers and release documentation to support the Early Science Program [RTN-011]. This report represents an opportunity to collectively exercise the practical aspects of developing documentation in compliance with the policies and guidelines for information sharing during commissioning [SITCOMTN-076].
- **Synthesize the new knowledge** gained from the ComCam on-sky commissioning cam-

paign to inform the optimization of activities between the conclusion of the ComCam campaign and the start of the on-sky campaign with the LSST Camera (LSSTCam).

- **Inform the Rubin Science Community** on the progress of the on-sky commissioning campaign using ComCam.

Other planned systems engineering activities will specifically address system-level verification ([LSE-29] and [LSE-30]) using tests and analysis from the ComCam campaign. While the analyses in this report will likely overlap with the generation of verification artifacts for systems engineering, and system-level requirement specifications will serve as key performance benchmarks for interpreting the progress to date, formal acceptance testing is not an explicit goal of this report.

The groups within the Rubin Observatory project working on each of the activities and performance analyses are charged with contributing to the relevant sections of the report. The anticipated level of detail for the sections ranges from a paragraph up to a page or two of text, depending on the current state of understanding, with **quantitative performance** expressed as summary statistics, tables, and/or figures. The objective for this document is to **summarize the state of knowledge of the system**, rather than how we got there or "lessons learned". The sections refer to additional supporting documentation, e.g., analysis notebooks, other technotes with further detail, as needed. Given the timelines for commissioning various aspects of the system, it is natural that some sections will have more detail than others.

The anticipated milestones for developing this interim report are as follows:

- 18 Nov 2024: Define charge
- 4 Dec 2024: First drafts of report sections made available for internal review
- 11 Dec 2024: Revised drafts of report sections made available for internal review; editing for consistency and coherency throughout the report
- 18 Dec 2024: Initial version of report is released

Warning: On-sky Pixel Image Embargo

All pixel images and representations of pixel images of any size field of view, including individual visit images, coadd images, and difference images based on ComCam commissioning on-sky observations must be kept internal to the Rubin Observatory Project team, and in particular, cannot be included in this report. Embargoed pixel images can only be referenced as authenticated links. See [SITCOMTN-076] for details.

2 System Performance Analysis

3 Active Optics System Commissioning

4 Image Quality

5 Data Production

6 Calibration Data

6.1 Twilight Flats

Because the flat field screen and illuminator is not expected to be operational while ComCam is on the telescope, we used dithered, tracked twilight flats to generate the combined flat calibration frames. The exposure time of the twilight flats were dynamically adjusted to hit a target count, generally in the range of 10-20k. The flats taken at a wide range of azimuth angles and rotator angles. See Fig. 1 for the counts per pixel per second as a function of sun elevation angle.

7 Science Pipelines Commissioning Observations

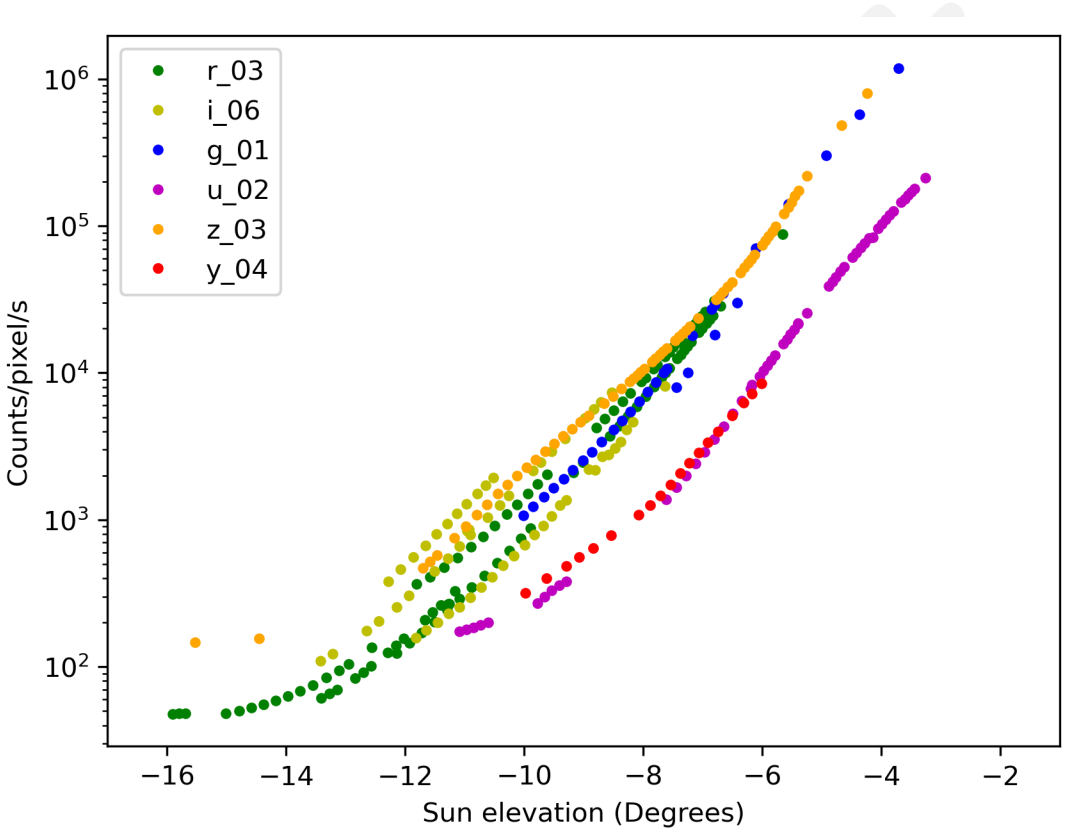

FIGURE 1: Twilight flat counts per pixel per second for each filter as a function of sun elevation angle.

8 Throughput for Focused Light

9 Delivered Image Quality and PSF

10 Instrument Signature Removal

The quality of the instrument signal removal (ISR) has improved during commissioning, as we create and deploy updated calibration products that better represent the LSSTComCam system. The following discussion summarizes our current understanding of a variety of features, both expected and newly seen on LSSTComCam, and presents our expected prognosis of the behavior of the full LSSTCam.

10.1 Phosphorescence

There are regions on some of the detectors (most visible in R22_S01, detector=1) which show bright emission, particularly at bluer wavelengths, as shown in Figure 2. This is believed to be caused by a thin layer of remnant photo-resist from the manufacturing process that remained on the detector surface, and is now permanent due to the subsequent addition of the anti-reflective coating. In addition to the large areas, there are also discrete point-source-like or cosmic-ray-like defects caused by accumulations of this material. Adding to the difficulty of mitigating these defects is that this photo-resist is known to be phosphorescent, explaining why these regions are more noticeable in the bluer filters.

The initial studies of this show that these features can continue to emit light up to several minutes after they've been illuminated. Due to the long duration of these features, we decided to place manual defect masks over the worst regions. The first of these manual masks takes up about 3.5% of that detector, smaller than but consistent with estimates that this would create a pixel loss of approximately one amplifier.

The ITL detectors in LSSTCam are believed to have been cleaned better, so this should be less of an issue on the full camera.

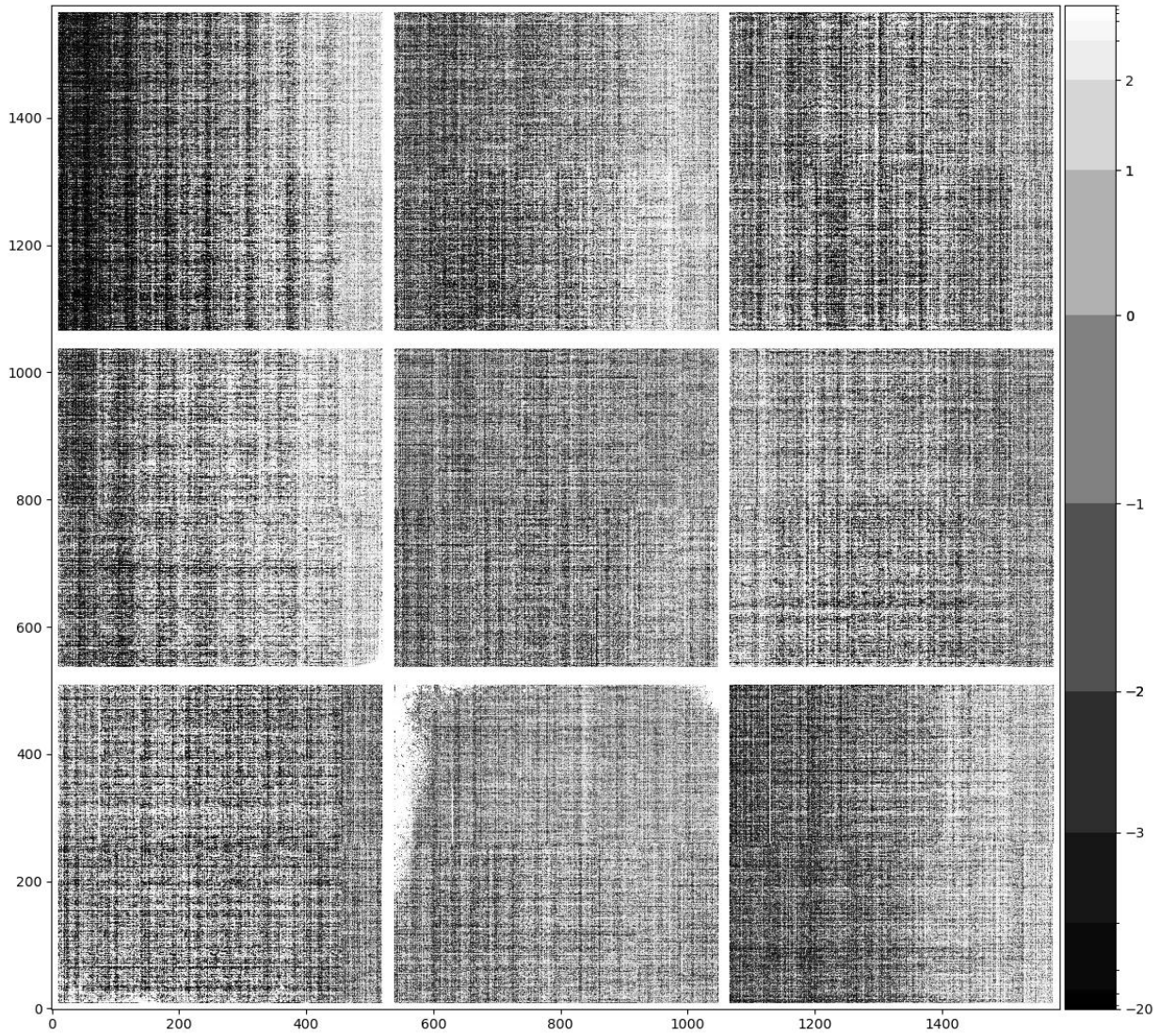

FIGURE 2: The phosphorescence seen in R22_S01, shown here in a dark exposure taken after a series of twilight flats (exposure=2024112000065). This material absorbs light at bluer wavelengths and re-emits that energy over a wide range of wavelengths.

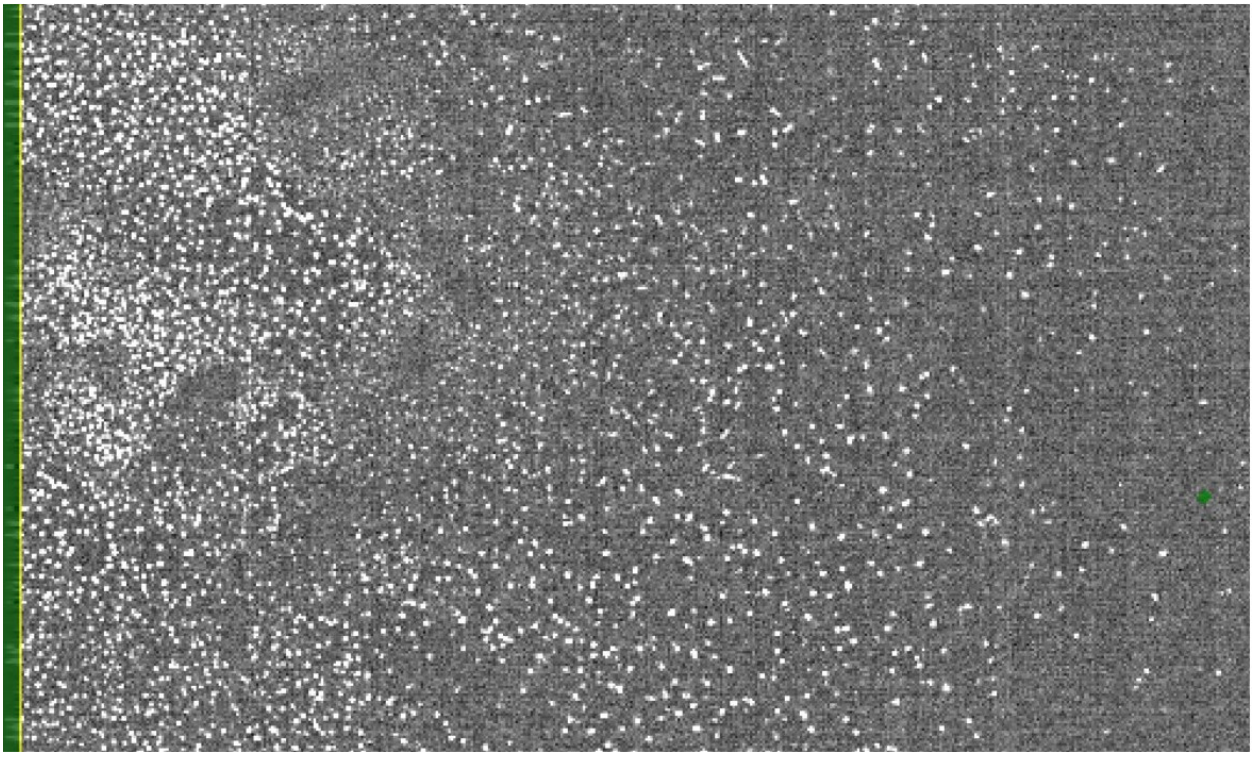

FIGURE 3: A full-resolution view of the edge of R22_S01. The features shown in this image are point-like sources caused by the trapped phosphorescence photo-resist.

10.2 Vampire pixels

There are defects on LSSTComCam that have been classified as "vampire" pixels, as they appear as a bright defect with a (generally) axisymmetric region surrounding the bright core, as if the defect is draining charge from its neighbors. The naming is at least broadly correct, as integrating to large radii shows that these regions do appear to conserve charge. There is an intensity dependence that makes these vampire pixels different than standard hot pixels, as these pixels do not show up on dark frames, only on flats and science exposures, where the detector surface is illuminated. After the initial discovery of the bright obvious vampires, we added new masking code that identifies the bright cores that are above 2.0 on the combined flat (pixels that are greater than 200% of the median flat level), and adds circular masks to the defect list. This appears to find the most problematic examples, but as we have improved flat quality during commissioning, we are finding that there is a sub-population that are not as severe, but likely have a similar physical mechanism. This population is still bright on the flat, with peaks around 1.2 (20% elevated relative to the flat), and may need to be masked as well. From an initial study in the lab, it appears that all ITL detectors on LSSTCam have a few of these kinds of defects, with two detectors approaching similar contamination levels as R22_S10 on LSSTComCam.

10.3 Saturated star effects

Although we expected to find saturated star trails coming from bright sources, the observed behavior of these trails is unique. Saturation spikes on most cameras appear as streaks extending from the core of the bright source along the direction of the parallel transfers, and truncate as the charge bleeds run out of charge (and can no longer overcome the potentials defining the pixel). The trails seem with LSSTComCam, however, extend the entire height of the detectors, crossing the midline break. These trails are also not at the expected high state, with the centers of these trails having flux levels lower than the average sky levels, creating dark trails. On the worst saturated objects, there is also evidence of charge pile-up near the serial readout, which can then create fan-like bright features at the edge of the detector. Those bright features can also then crosstalk onto other amplifiers.

The underlying physics is not well understood, and further study will be needed to see if we can correct these trails outside of the regions of charge buildup. Until we have a correction, we plan to begin masking both the trail and the fan-spread near the serial register.

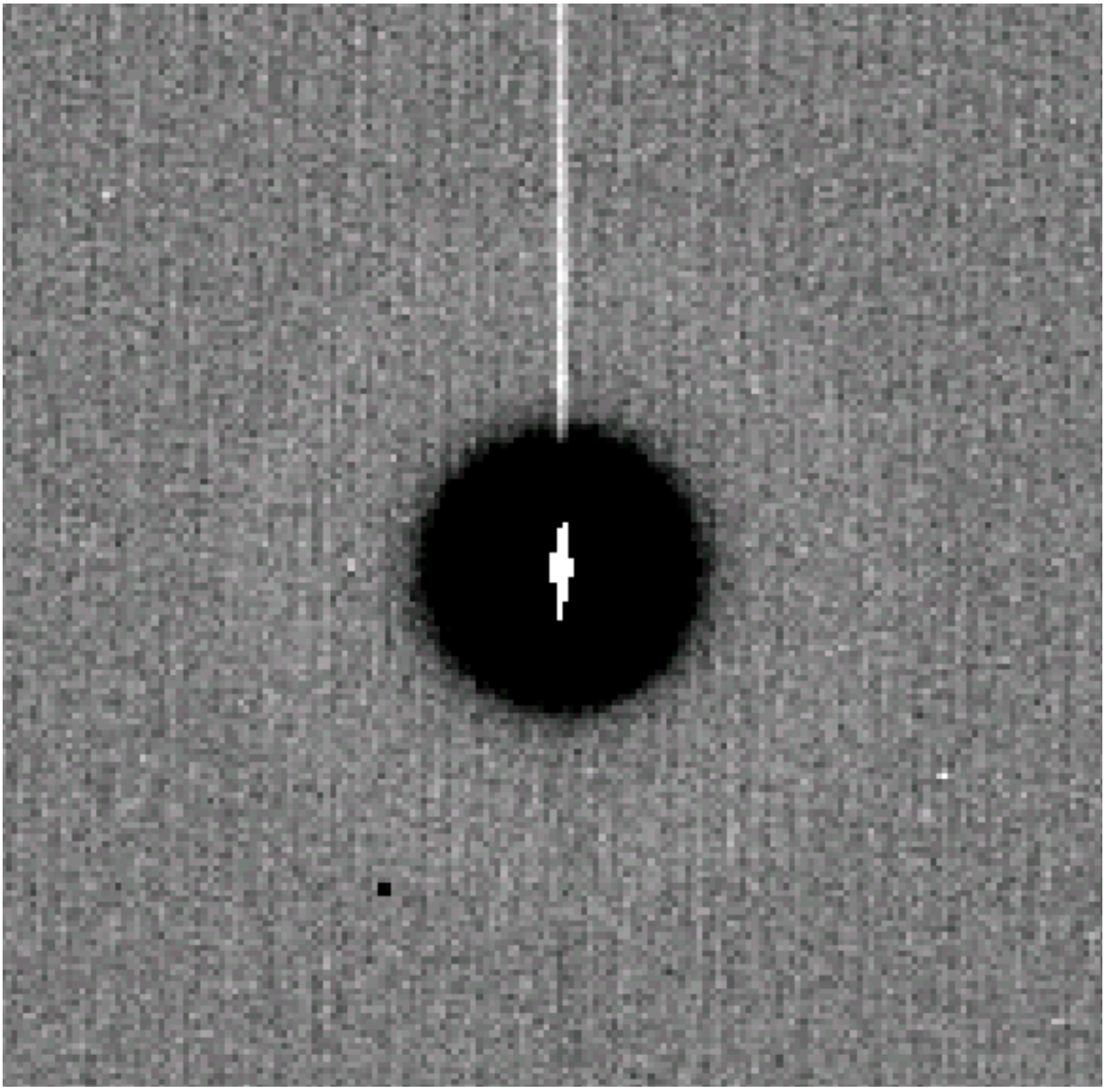

FIGURE 4: A close up of one of the largest vampire pixels. The bright core and region of depletion are clearly visible. Currently we only mask the core and depleted region, but will be extending this to mask the persistence-like trail that this feature leaves in the next few weeks.

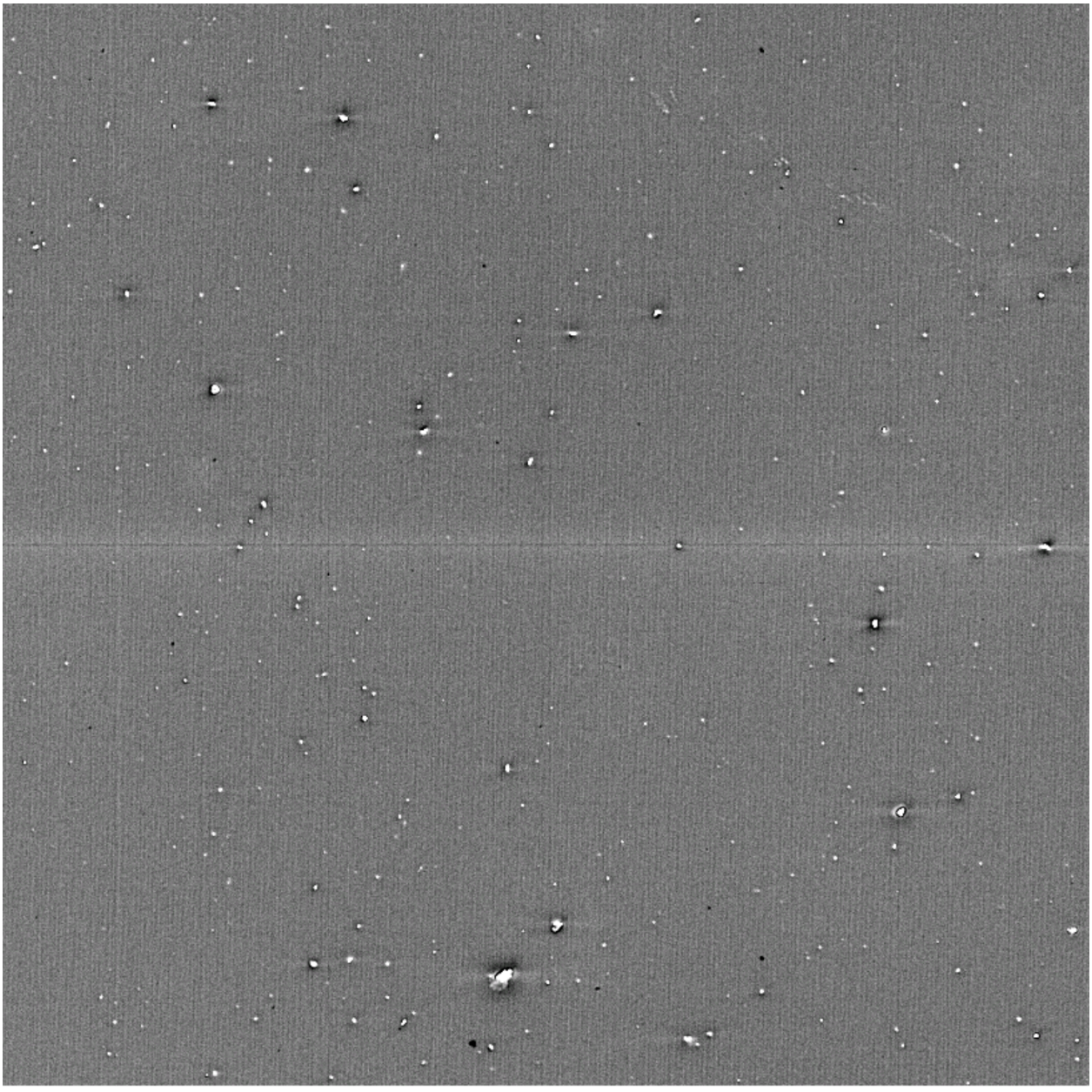

FIGURE 5: A view of detector R22_S10 in y-band, which has a large number of less significant vampire pixels.

Although we haven't seen identical features on LATISS, the presence of these odd trails on all LSSTComCam detectors suggests that this is a property of the ITL devices, and so will likely be seen on LSSTCam as well.

10.4 Gain ratios

LSSTComCam has been the first large-scale application of the updated "IsrTaskLSST" task, which uses a model of how the various signals combine to form the raw images to inform how we correct those signals during the ISR process. One improvement of this new task is that we now apply per-amplifier gains before flat correction, removing the gain component that was previously included in the flat correction. This results in the flat containing mainly QE and illumination patterns, which is much "flatter" than flats that also include gain terms (which offset the amplifiers relative to each other).

If we have properly diagonalized the flats and the gains, we would expect that applying the gain correction would create images with consistent sky levels across different amplifiers. However, when we look at images taken on-sky, our initial gain values result in some amplifiers being significantly different than their neighbors. The gains that we use are derived from the photon transfer curve (PTC), which uses flat pairs at different flux levels to monitor the properties of the noise. We have two of these sequences taken in the lab, and they disagree at the few percent level. This is similar in scale to the errors necessary to explain the on-sky differences. Further complicating this issue, the offsets seen in twilight data (used for flats) and that seen during the night also seem to differ. These differences so far have not been found to correlate with any device temperature, time, or voltage values. The gain correction fix appears to be stable, as we've only needed to generate and apply it once.

10.5 Crosstalk

We are currently using crosstalk values that were constructed by averaging the lab-based ITL measurements taken on LSSTCam. These are working better than expected, with residuals post correction being only a few electrons peak to peak. We plan to do a more complete crosstalk study using on-sky data, but the current results suggest that these lab measurements are sufficient for LSSTComCam, and expect the same to be true for LSSTCam.

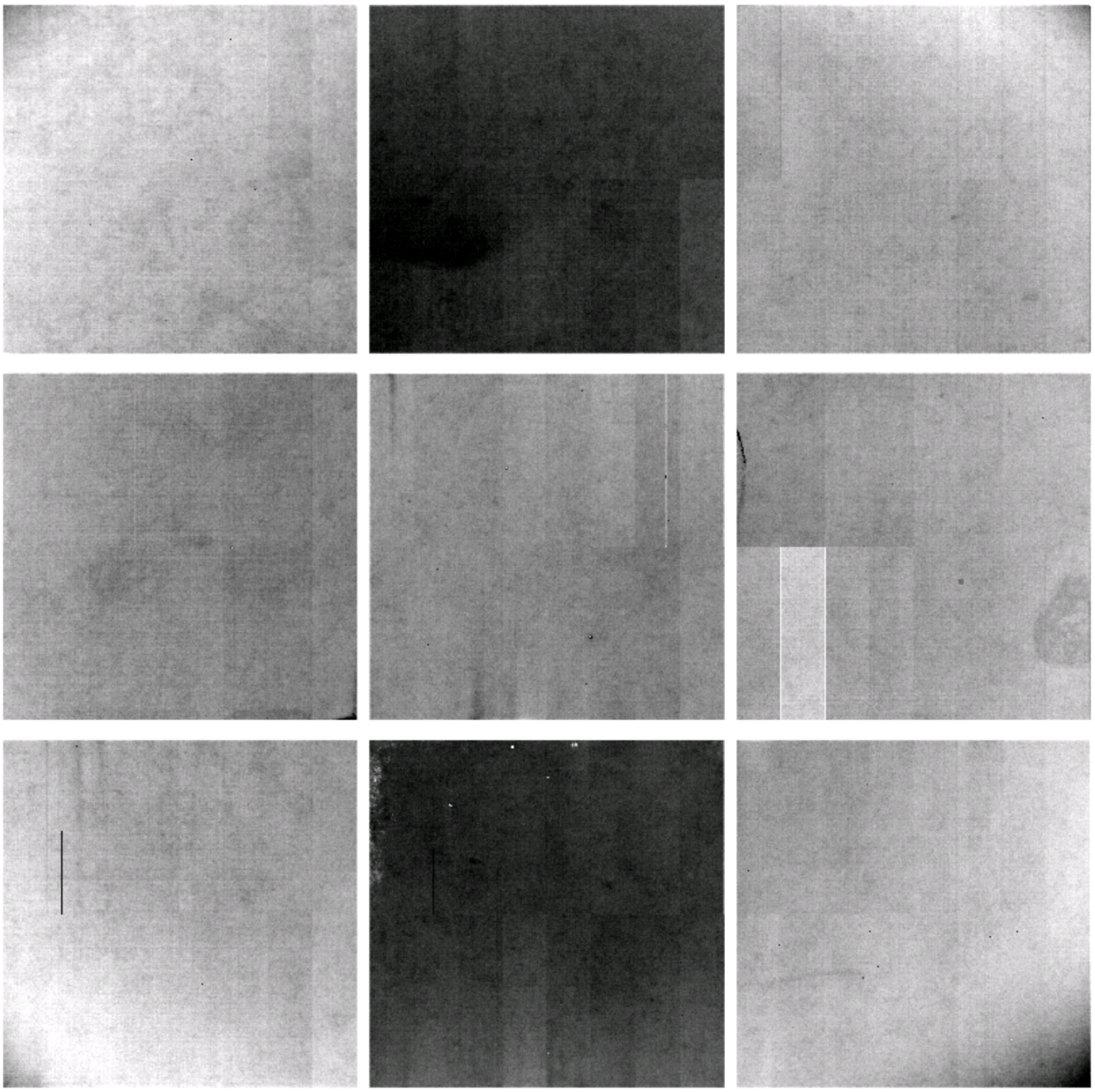

FIGURE 6: The ratio of the twilight-flat divided by a flat constructed from 94 r-band science frames. The scaling ranges from 0.9905 to 1.007. The visibility of amplifiers is caused by the unknown gain errors. The bottom right corner amplifier (C07) on R22_S21 is one of the indicator amplifiers, as it diverges from its neighbors. Although the C00-C03 amplifiers in R22_S12 also show significant offsets, these amplifiers also have an unrelated CTI issue, making them less reliable indicators.

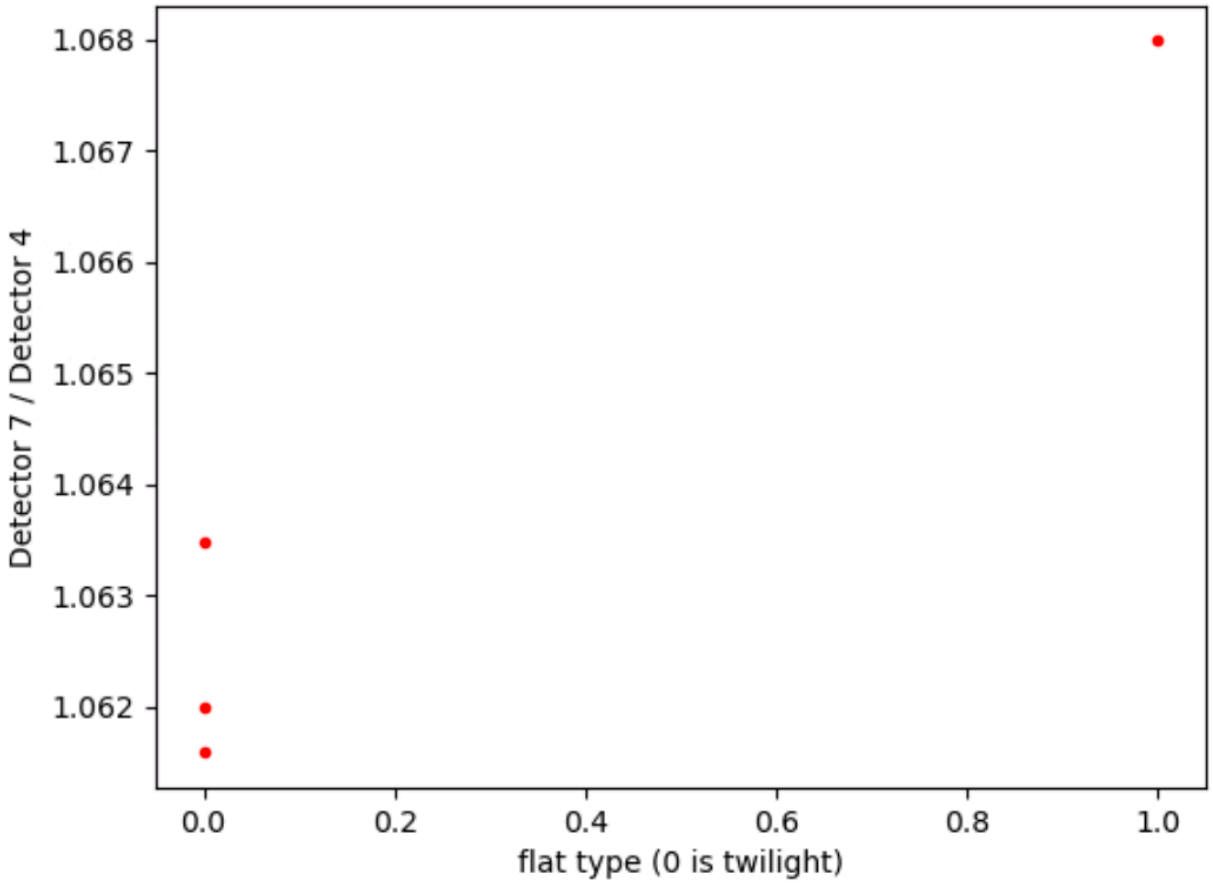

FIGURE 7: A comparison of the gain ratio between amplifiers in R22_S12. C07 is chosen as the indicator amplifier, and C04 is the reference. We have three twilight flat measurements taken at different rotator angles, and one from the 94 input sky flat.

10.6 Twilight flats

There is no flat screen currently available for the main telescope, and so we have constructed twilight flats for all bands using exposures taken to have median counts between 15000-20000 ADU. We have some dithering in the inputs, which have allowed us to reduce the impact of stars that print through into the flat. This reduction of non-sky signals is imperfect, and the current i-band flat shows a satellite trail as a result We are working to replace this flat using newly taken data.

10.7 Operations

The Telescope and Auxiliary Instrumentation Calibration Acceptance Board (TAXICAB) has been meeting previously to discuss LATISS calibrations, and has been helping manage calibrations for LSSTComCam. This process has not prevented problematic calibrations from being deployed (like the i-band flat with the satellite trail), but it has ensured that multiple people have checked some set of results. We are generating calibration verification reports regularly as part of this process (available at `https://s3df.slac.stanford.edu/people/czw/cpv_reports/`), and plan to add new metrics and checks to these as we discover more features of these detectors.

11 Low Surface Brightness

12 Astrometric Calibration

13 Photometric Calibration

We have started commissioning the full photometric calibration pipeline for Rubin Observatory, with great success so far. For testing photometric calibration we have obtained over 150 dithered science observations in ugriz over the Extended Chandra Deep Field-South (ECDFS) (one of the planned LSST deep fields), and tens more in rizy over the Euclid Deep Field South (EDFS). All of the science data has delivered seeing of ~ 0.8 to ~ 1.5 arcsecond seeing. The validation work in this document covers the ECDFS field with more complete filter coverage.

The precision photometric calibration software used for Rubin is the Forward Global Calibration Method (Burke, Rykoff, et al. 2018) which was used successfully to achieve better than 2 mmag uniformity for the Dark Energy Survey. This software has been adapted for the LSST Science Pipelines and has been used on Hyper Suprime Cam Special Survey Program (HSC SSP) for data releases since DR2.

The performance on HSC data has not been as good as that on DES data due to a number of reasons, yielding repeatability and uniformity closer to the 5 mmag level for grizy data. First, we have had a lot of problems with HSC backgrounds and amp-to-amp non-linearities. Second, the HSC survey strategy was not well suited to self calibration due to the slow slewing of the telescope and the long time required to change a filter, leading to lots of isolated single-band single-night surveys. Third, we do not have detailed throughput scans including detector-to-detector QE variations and in-situ scans of the significant filter variations that are required for the full forward modeling in FGCM.

Early calibration of the ComCam data is in many ways easier than that of HSC. First of all, we have a smaller camera (9 detectors) and thus fewer variations to have to cross-calibrate. Second, the camera is situated in the center and easiest to calibrate part of the focal plane. Third, we only have one field to calibrate across a few nights of data so far over a limited range of airmass. Fourth, the survey strategy (multiple bands per night dithered and repeated with overlapping filters from night to night) is well suited to self-calibration. On the other hand, we do not have the CBP set up yet, so we do not have detailed filter or detector scans available for ComCam, and are just using the LSSTCam reference filter throughputs and average detector throughput for the LSSTCam ITL detectors. In addition, we do not have a flat field screen so we have had to rely on twilight flat observations for flat fielding.

13.1 Processing Overview

We start with the standard ISR as documented in Section 10. While there are a number of challenges that we have discovered with the ITL detectors, these are mostly near the sky level, while the testing of photometric calibration is focused on brighter stars that are less affected by these issues. We then apply twilight flats, which we are investigating how to make better. At the same time, we are going to have the flat field screen and laser and projector installed prior to the commissioning of LSSTCam, so we do not want to spend too much time worrying about specific challenges of twilight flats which are only necessary for ComCam.

After flat fielding we find an initial point-spread function (PSF), do a star selection based on source and psf moments that was developed for HSC single-frame processing, and perform an initial astrometric solution and photometric solution (with a single zero-point per detector). The initial astrometric solution is used to associate star observations together prior to global photometric calibration with FGCM. The initial photometric solution is used for rapid analysis and prompt processing, but is not used at all for FGCM which relies entirely on instrumental fluxes (in units of electrons) with a minor constraint from the reference catalog.

13.2 Global Photometric Calibration with FGCM

All associated stars with observations with signal-to-noise greater than 10 are input into the FGCM solution. In addition, reference stars from The Monster reference catalog are associated with the stars . Only a small fraction of the reference stars are used in the FGCM solution, sufficient to estimate an "absolute" calibration (trusting that The Monster is a good absolute reference catalog). There is additional ongoing work with absolute calibration with respect to the CalSpec star C26202 which is not saturated in LSST images and is fortunately contained in ECDFS that is described below.

The FGCM model constrains the atmospheric parameters per night, as well as the absolute throughput relative to the input scans. The standard atmosphere is given by MODTRAN, run at the elevation of Cerro Pachon at airmass 1.2 with an Angstrom aerosol model. The optics and filters are all taken from *lsst/throughputs* version 1.9, and the detector throughput is taken from the ITL average of the lab scans ingested into *obs_lsst_data*. Note that the detector QEs are normalized to 1.0 at 800 nm, which is certainly greater than the true QE at this wavelength.

13.3 FGCM Results on the ECDFS Field

The FGCM results presented here are based on the `LSSTComCam/runs/DRP/20241101_20241113/w_2024_46/DM-47566` DRP processing run, specifically the 157 visits overlapping tracts 4847,4848,4849,5062,5063,5064 which are in the ECDFS field. Specifically there are 28, 18, 38, 45, 28 visits in ugriz respectively. All QA plots are available in the plot navigator at https://usdf-rsp.slac.stanford.edu/plot-navigator in the collection `u/erykoff/LSSTComCam/DM-47303/test2/build2/run9`. In this section we focus on some of the highlights.

Note that FGCM defines a "photometric" observation as one that is consistent with the forward

model, including normal variations in the atmosphere, airmass, known detector throughputs, filter curves, and additional accomodation for aperture corrections (discussed in Burke, Rykoff et al). With this definition fully 92% of the observations were deemed to be photometric by the code.

13.3.1 Illumination Corrections

Part of the FGCM solution is generating illumination correction maps, with a second-order 2D Chebyshev polynomial over each detector. Prior to LSSTCam commissioning this will be turned into a separate calibration product generated from dense dithered star field observations (Y1) or from the CBP (future years). We have not yet done dithered observations with ComCam over a dense field, only high latitude, which limits the precision. Nevertheless we are able to constrain reasonable illumination corrections. The offsets from detector to detector in the illumination correction are due to unexpected offsets in the twilight flats that we are investigating.

13.3.2 Photometric Repeatability

The photometric repeatability after the FGCM fits was excellent. We show here the repeatability histograms, after all chromatic corrections, for the stars used in the fit ("all stars"). Although 10% of the stars are reserved, the histograms do not yet have good statistics. These plots are all made with signal-to-noise greater than 100 stars (with better than 1% photometric errors). Therefore the scatter is often dominated by photometric error. The label "sigma_fgcm" is meant as an estimate of the intrinsic scatter after subtracting off the photometric error in quadrature. The plots are split into four panels, showing all stars, the 25% bluest (from $g - i$ color), the 50% middle color, and the 25% reddest stars. Note that the reddest stars tend to be fainter and thus have larger photometric error. Furthermore, there are no red stars observed in the u-band. In all cases except the u-band the intrinsic repeatability is 1 mmag or better, and for the u-band it is better than 5 mmag, comfortably exceeding our requirements.

13.3.3 Detector Chromaticity Fits

In the absence of full in-situ throughput scans, we additionally constrain the "chromaticity" of the detectors, which is a first-order adjustment to the slope of the peak of the throughput curve per-detector. By doing this adjustment in throughput space rather than color space we

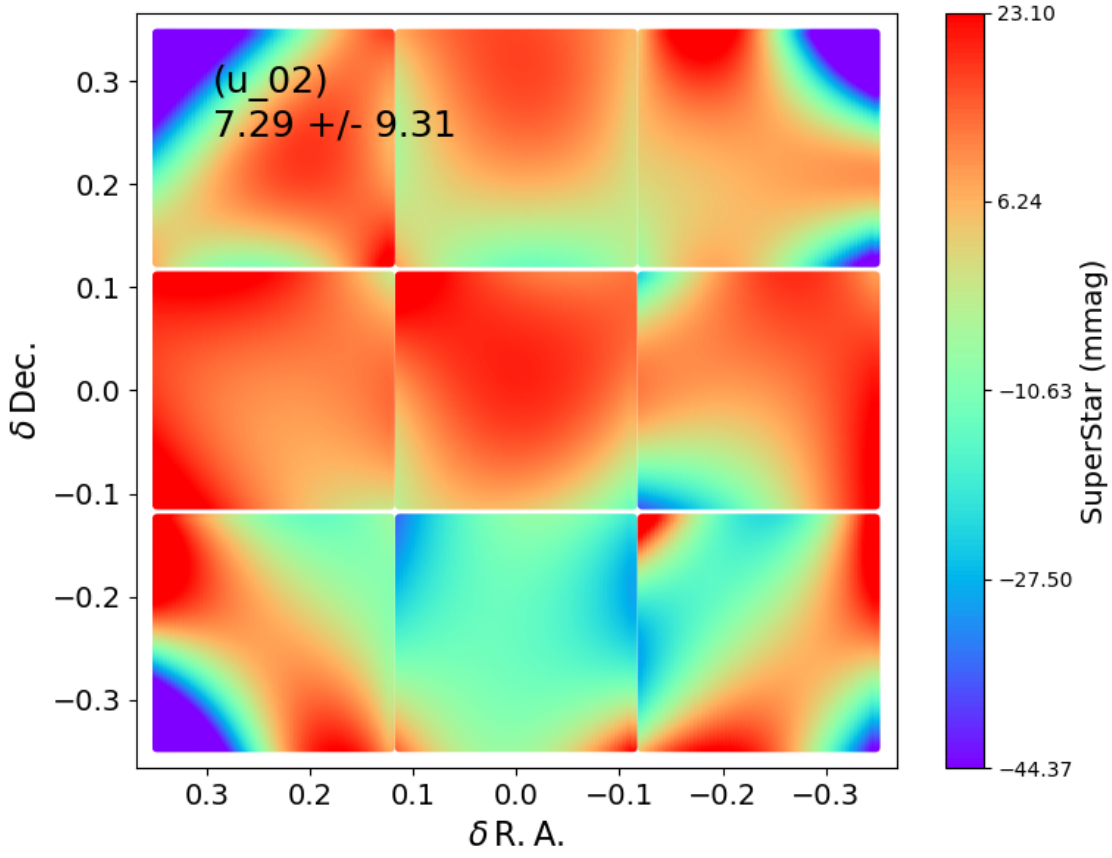

FIGURE 8: Illumination correction derived from FGCM for the u band.

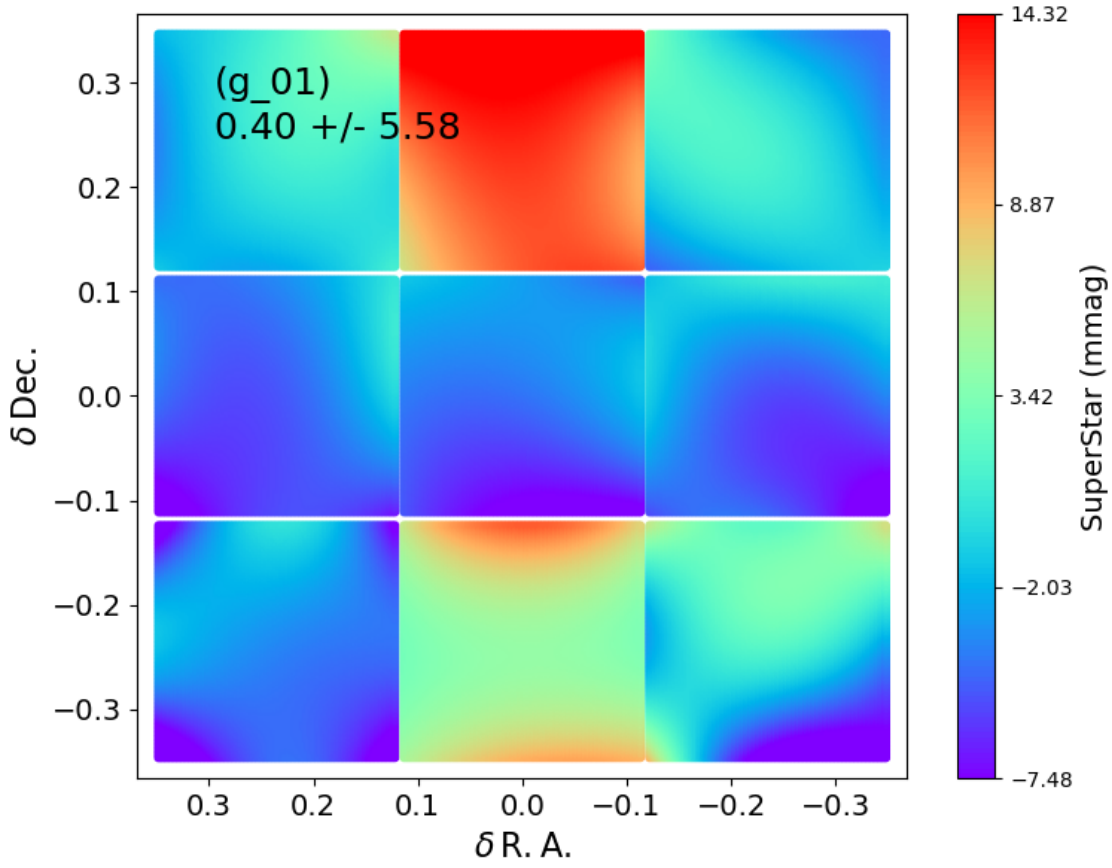

FIGURE 9: Illumination correction derived from FGCM for the g band.

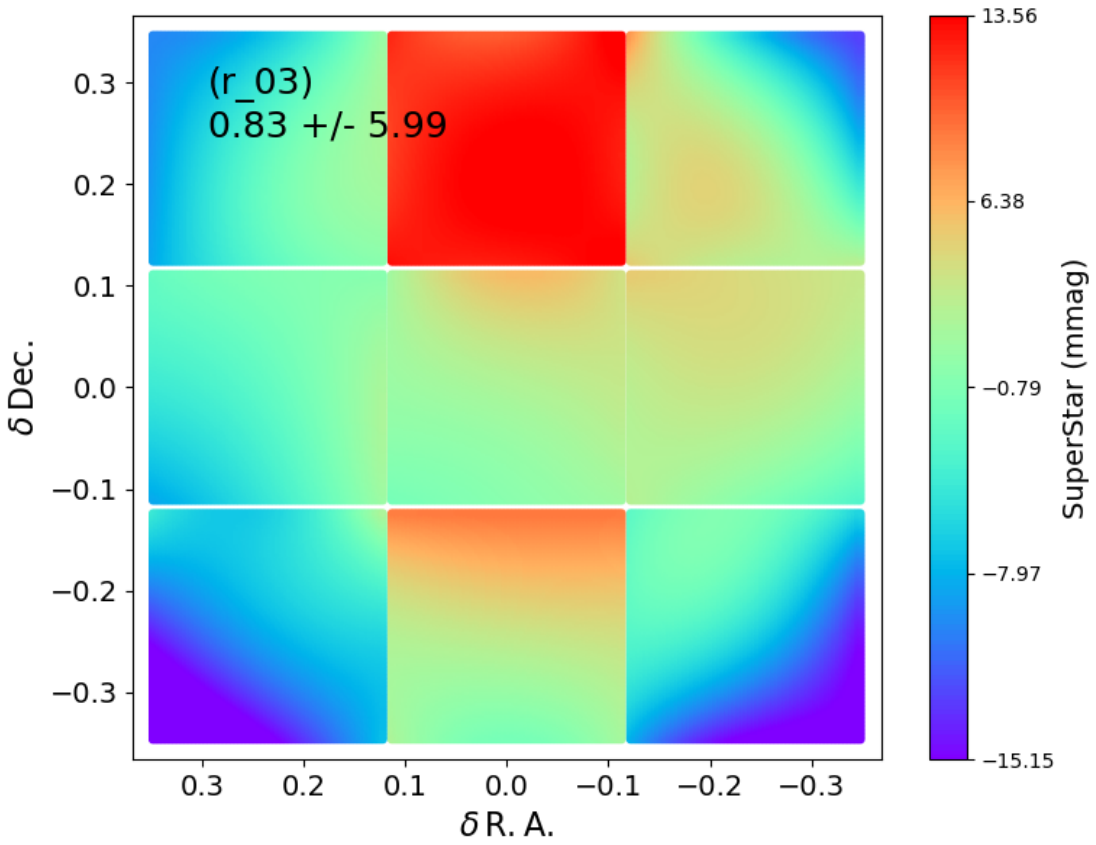

FIGURE 10: Illumination correction derived from FGCM for the r band.

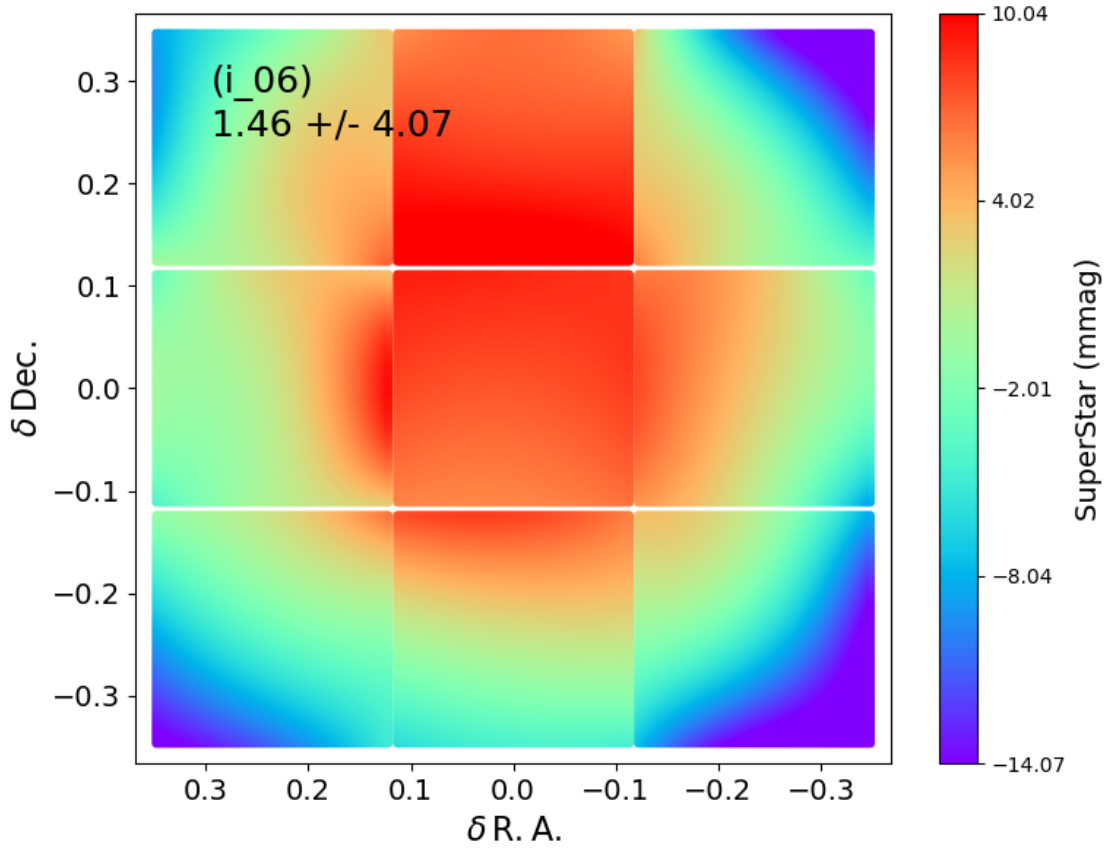

FIGURE 11: Illumination correction derived from FGCM for the i band.

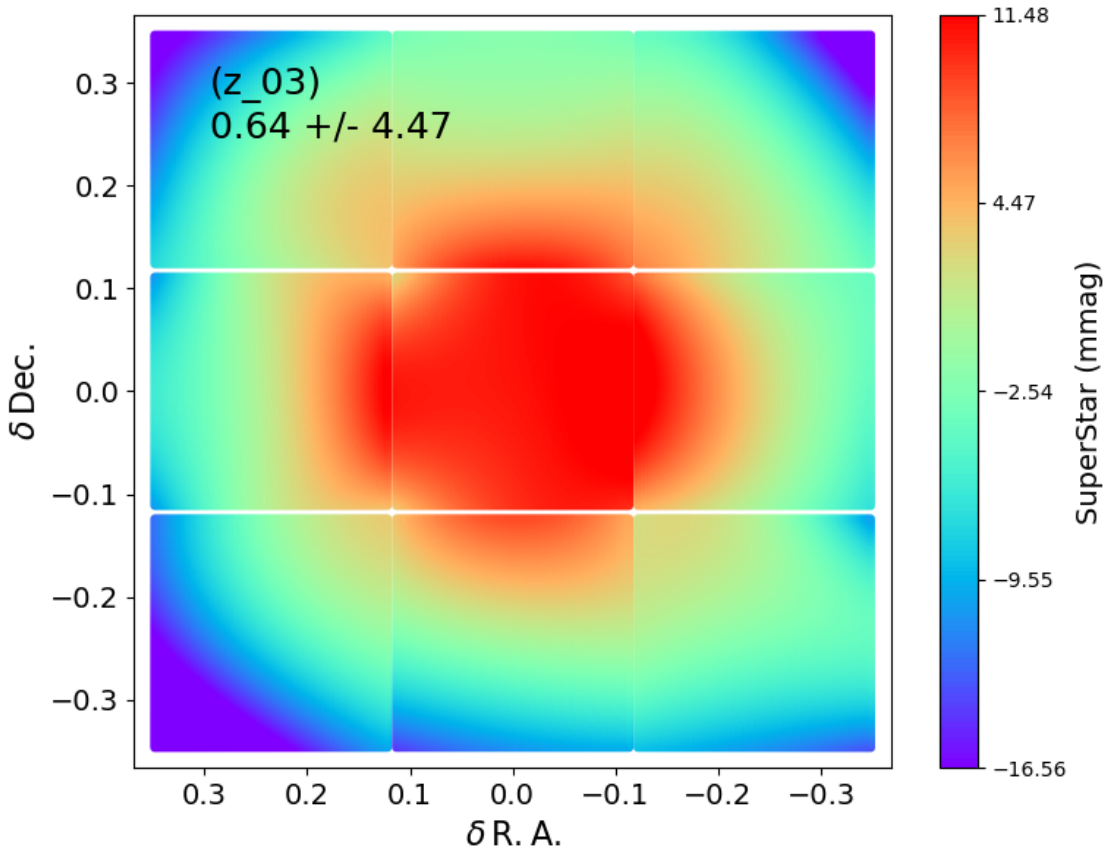

FIGURE 12: Illumination correction derived from FGCM for the z band.

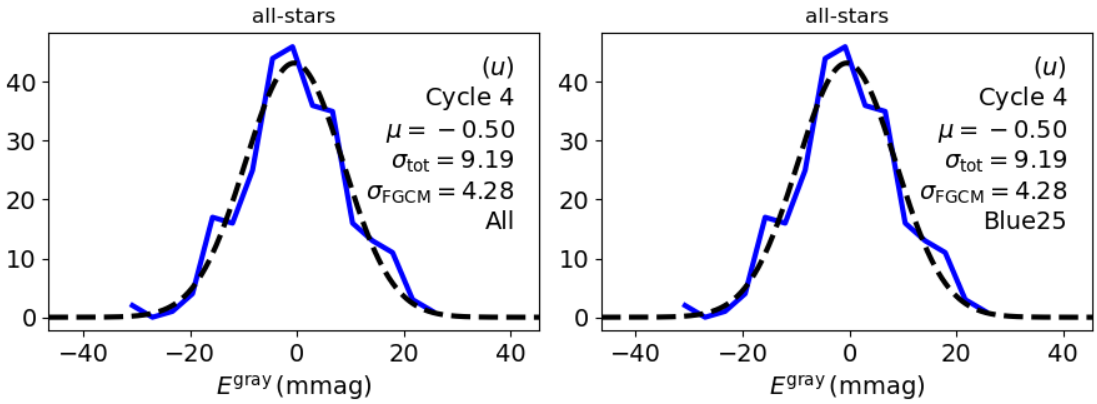

FIGURE 13: Photometric repeatability for stars in the u band.

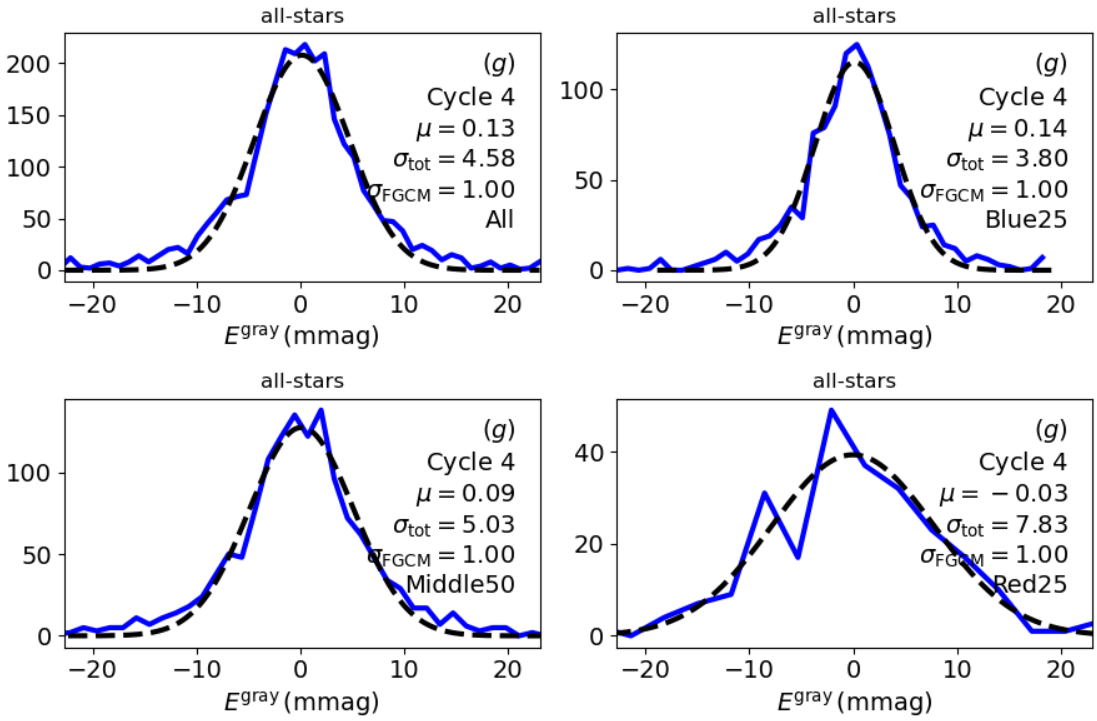

FIGURE 14: Photometric repeatability for stars in the g band.

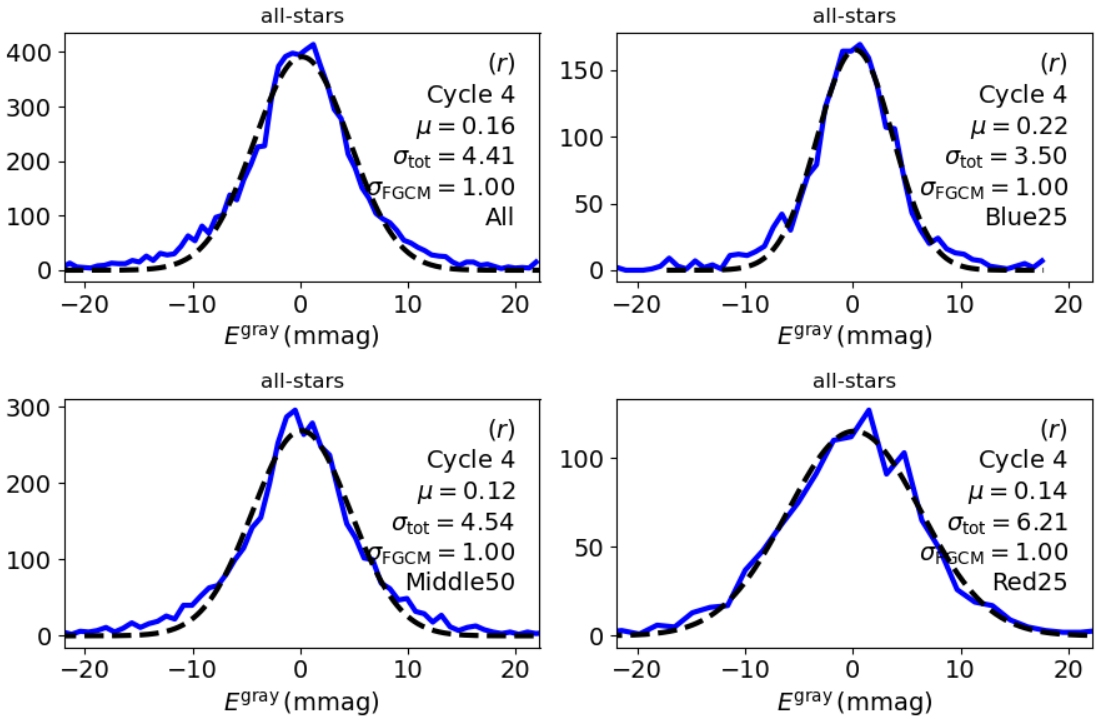

FIGURE 15: Photometric repeatability for stars in the r band.

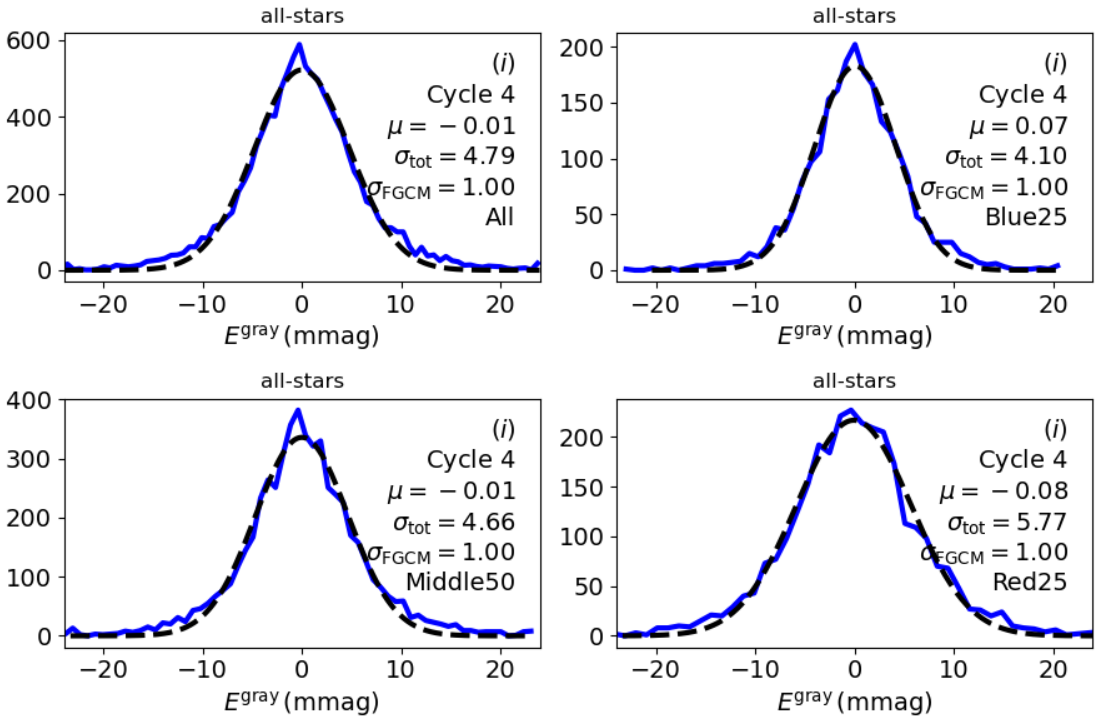

FIGURE 16: Photometric repeatability for stars in the i band.

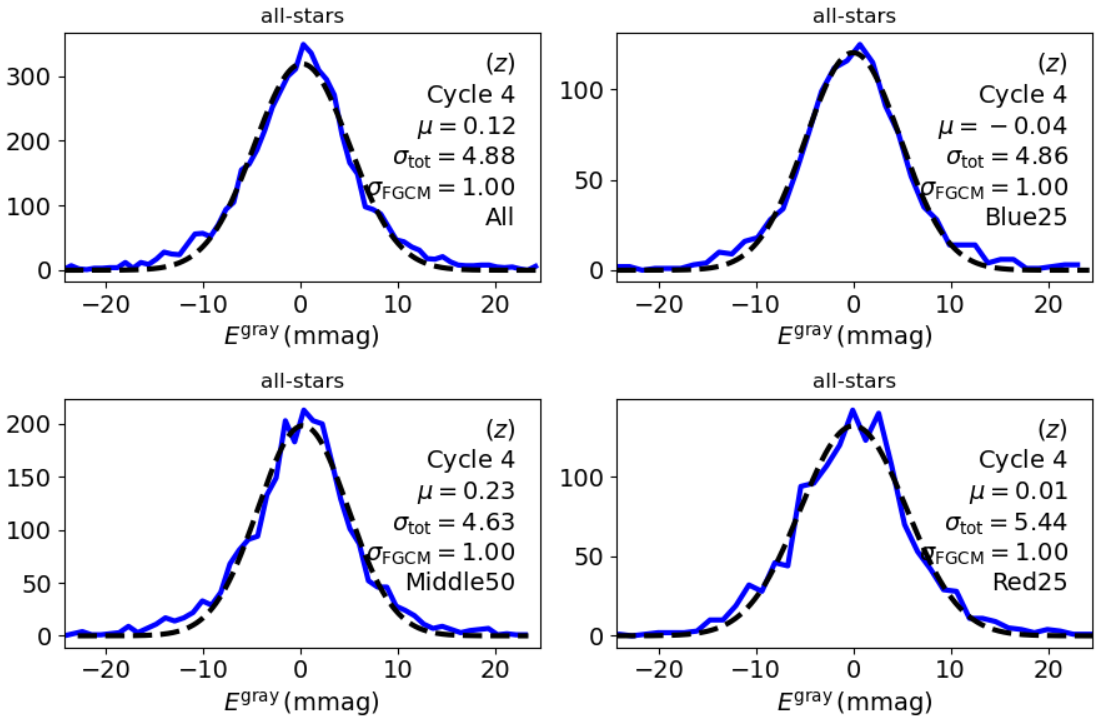

FIGURE 17: Photometric repeatability for stars in the z band.

can preserve the forward model approach, and additionally apply these corrections to any SED. Note that this operation assumes that the filters are perfectly known, and it is only the detector throughput that is varying. This is, in general, a valid assumption in the g band where the AR coating varies from detector to detector causing chromatic differences in this band.

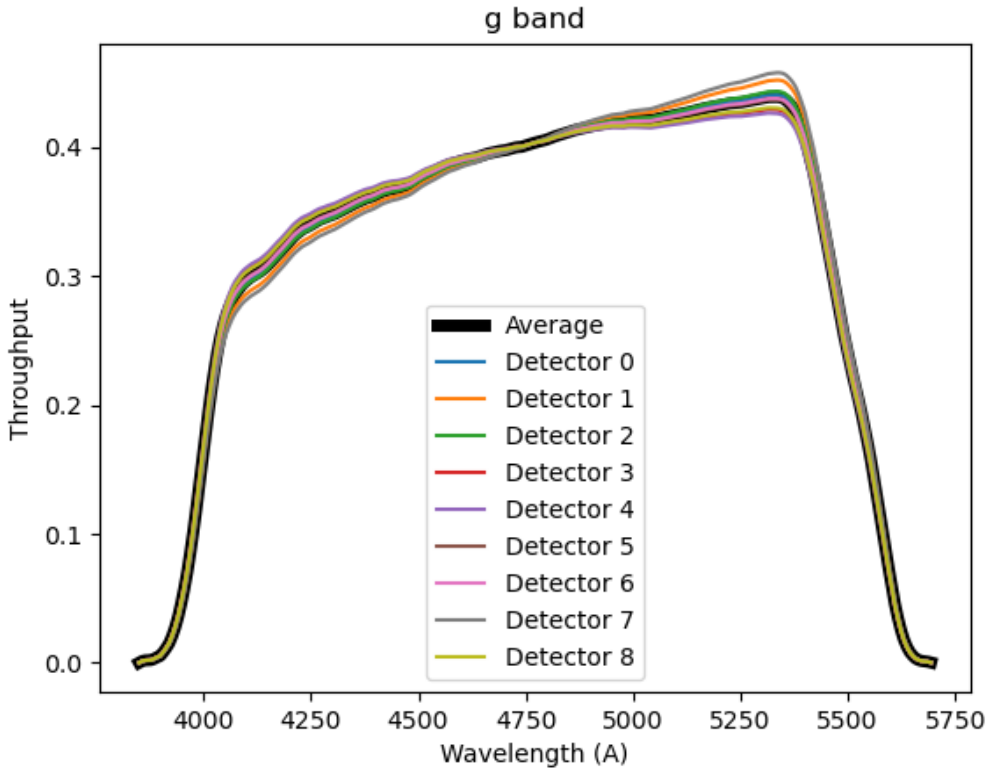

FIGURE 18: Variation in throughput in the g band for the 9 ComCam detectors as derived from star colors. These are all constrained relative to the average ITL throughput. The CBP will be used for making this measurement "correctly", but this serves as a prediction of what variations the CBP scans should observe if we have it running on ComCam.

13.3.4 Absolute Throughputs

The FGCM fit performs a "dead reckoning" of the expected absolute throughput given the telescope aperture, the effective gain, the standard atmosphere, and the various throughputs input. See above for the throughputs assumed. If we trust The Monster reference catalog for absolute calibration, Figure 19 shows the comparison of the delivered throughput to the predicted throughput. In griz bands it is very close, given that (a) we know that the peak detector QE is not 100%; and (b) the ComCam front lens did not have an AR coat applied, thus

reducing its throughput relative to nominal LSSTCam lenses. In u band we are getting more throughput than predicted. This may be an issue with the reference catalog, or our ComCam u-band QE is 20-30% larger than the baseline expectation. Given how fast the detector QE falls off in the u-band, it would not take much to increase the throughput by this factor.

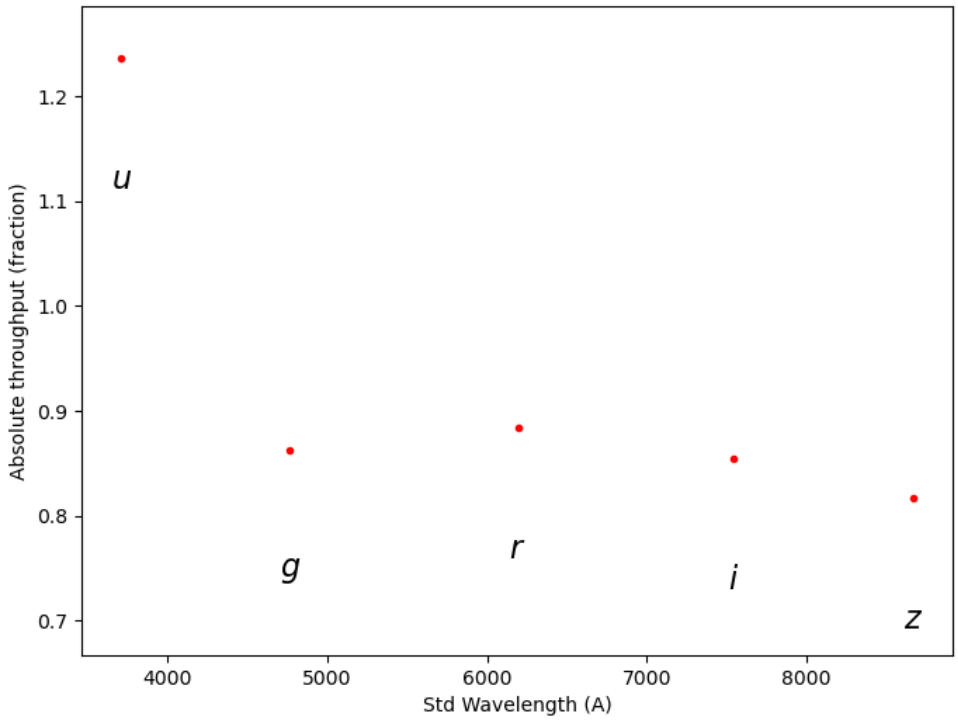

FIGURE 19: Absolute throughput derived per band, relative to naive expectations.

We have additional ongoing studies of absolute throughputs using the CalSpec standard C26202 directly.

13.3.5 Comparison to The Monster

Given our calibrated stars from the FGCM fit we can compare the magnitudes as a function of color against The Monster reference catalog. The "lsst" fluxes in The Monster were derived by using stellar spectra to convert from The Monster native DES system to the standard throughputs in lsst/throughputs v1.9. These do not match ComCam, in particular it used a strange hybrid of ITL/E2V for the detector throughput, which is not correct for ComCam. Therefore,

we do expect residual color terms. Studies are ongoing on whether these color terms are expected given the differences between the ComCam throughput and the predicted LSST throughput. Further validation will be possible if we get CBP scans prior to the removal of ComCam.

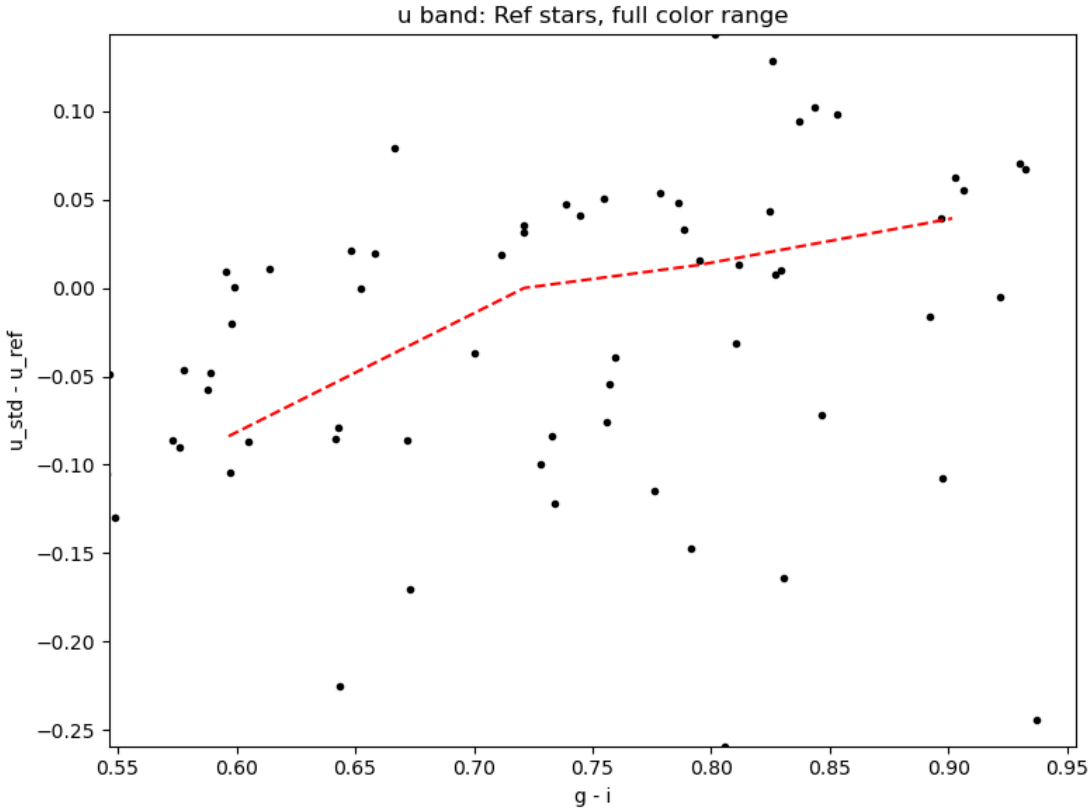

FIGURE 20: Residuals between FGCM standardized magnitudes and The Monster predicted LSST magnitudes for the u band as a function of $g - i$, assuming The Monster has the correct absolute throughput.

13.3.6 Background Oversubtraction

As a side-effect in the calibration, FGCM tests local background oversubtraction by looking at the statistical difference between two large aperture magnitudes. If the background were perfectly measured then the difference in magnitude will just be a measure of the wings of the PSF (a local portion of the growth curve) which should be self-similar for all star fluxes. Instead, we generally see a downturn consistent with a constant background offset. This background oversubtraction has been seen in DES, HSC, and ComCamSim data at similar

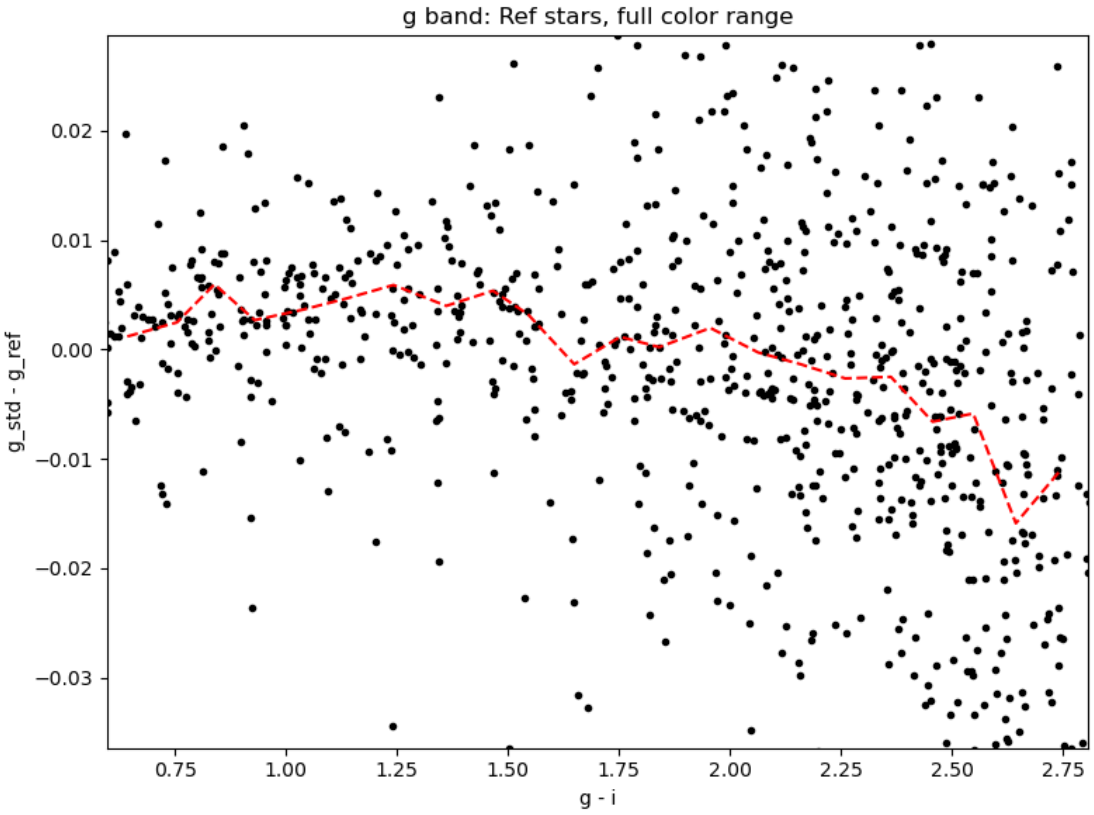

FIGURE 21: Residuals between FGCM standardized magnitudes and The Monster predicted LSST magnitudes for the g band as a function of $g - i$, assuming The Monster has the correct absolute throughput.

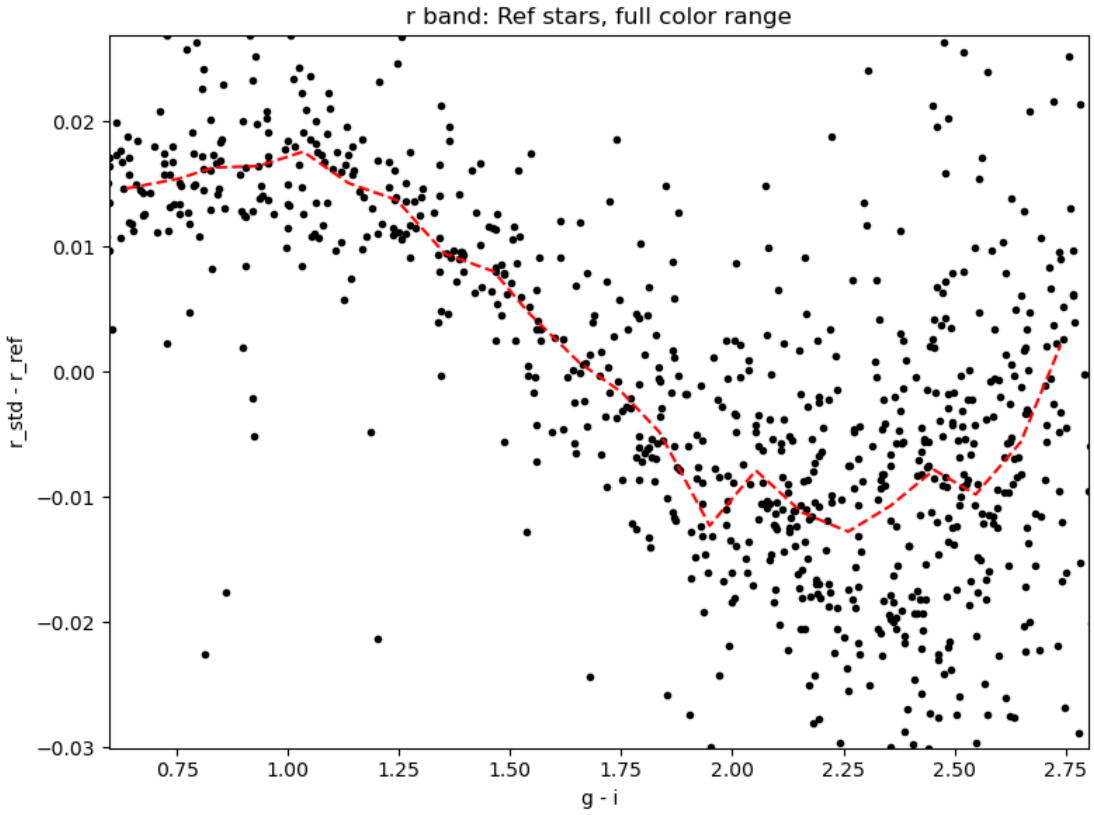

FIGURE 22: Residuals between FGCM standardized magnitudes and The Monster predicted LSST magnitudes for the r band as a function of $g - i$, assuming The Monster has the correct absolute throughput.

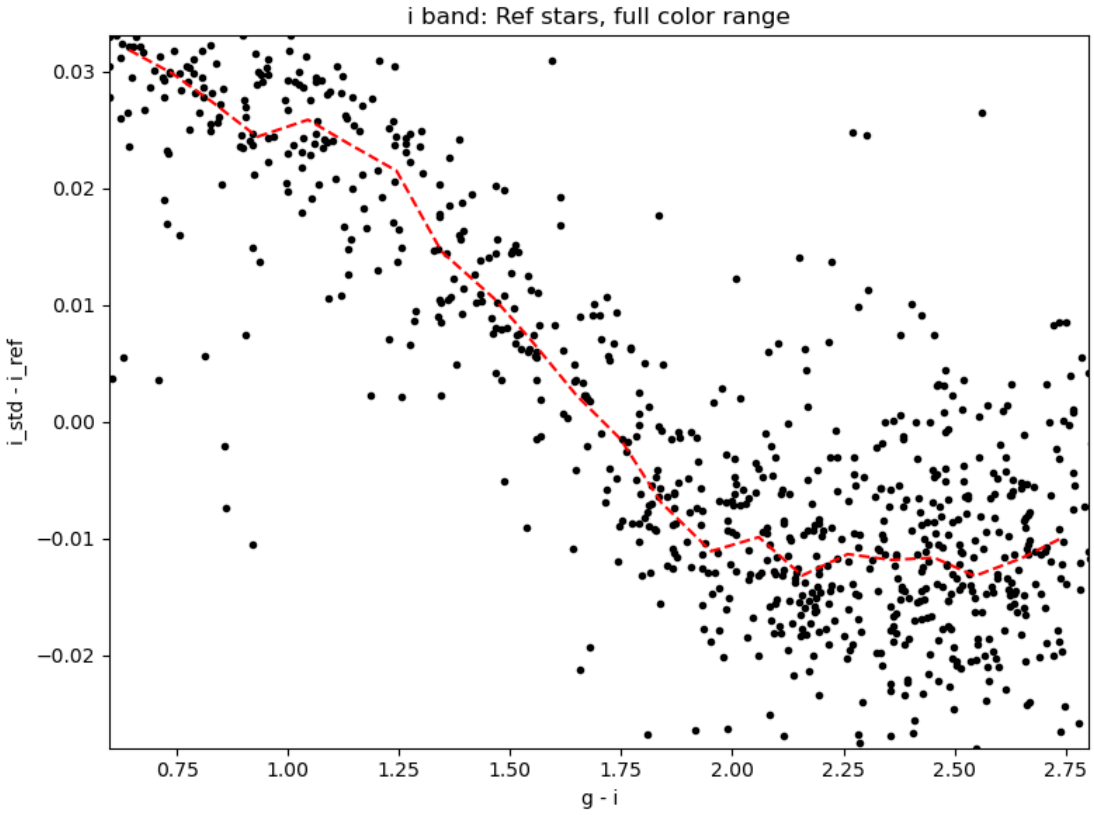

FIGURE 23: Residuals between FGCM standardized magnitudes and The Monster predicted LSST magnitudes for the i band as a function of $g - i$, assuming The Monster has the correct absolute throughput.

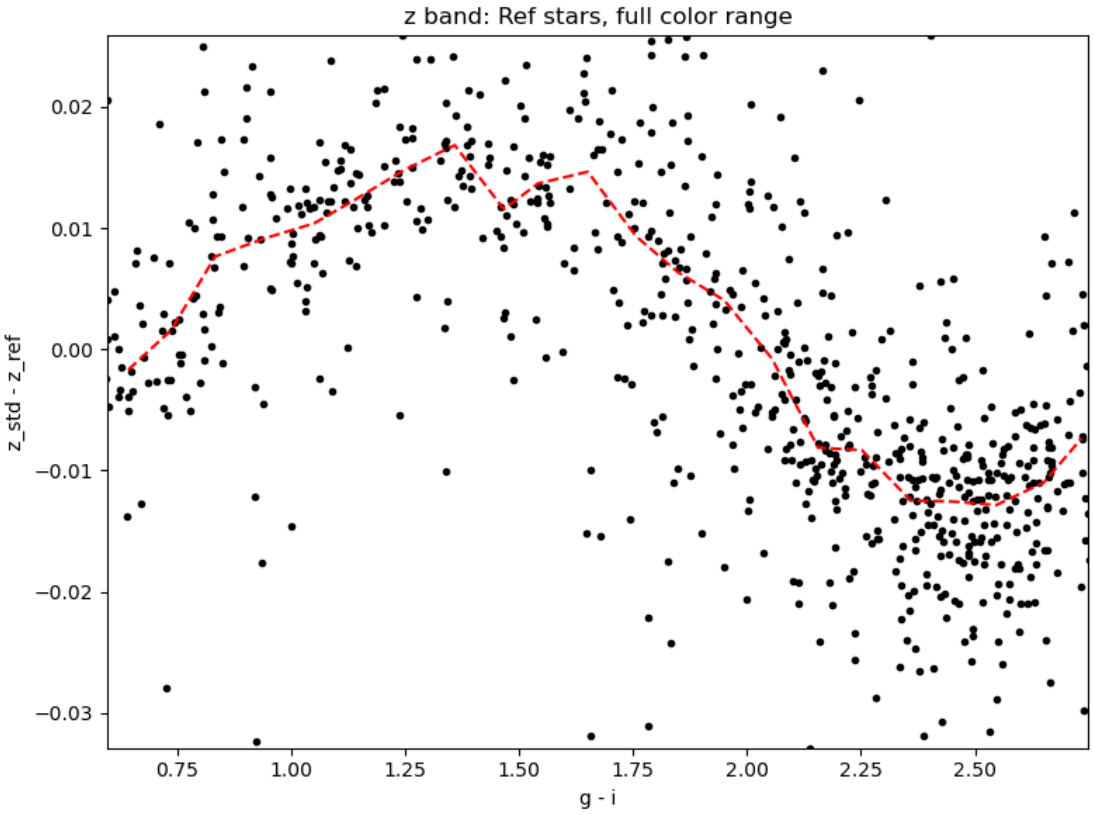

FIGURE 24: Residuals between FGCM standardized magnitudes and The Monster predicted LSST magnitudes for the z band as a function of $g - i$, assuming The Monster has the correct absolute throughput.

levels with different photometric pipelines. It is worse in the redder bands. It seems to be caused by the far wings of stars (in DES all stars and galaxies brighter than 17th magnitude in i contribute), as well as possibly due to faint undetected sources. This same background oversubtraction effect is seen in the ComCam images. Further investigations are being done by the low-surface-brightness science unit.

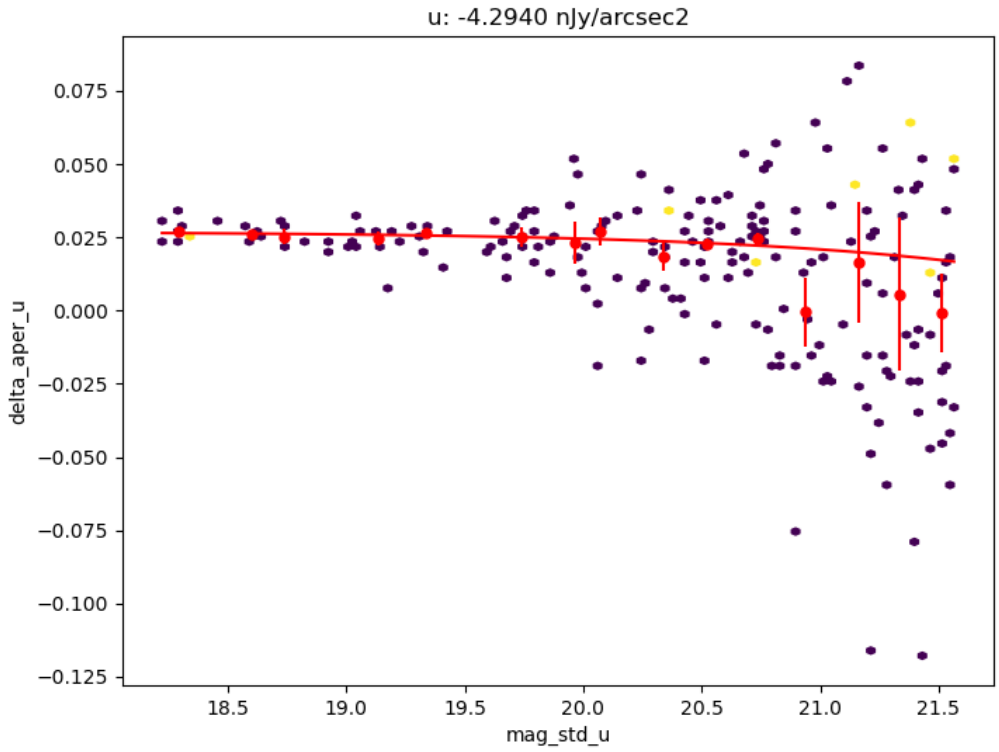

FIGURE 25: Estimate of the background oversubtraction using delta magnitudes from large apertures in the u band. The amount of curvature is a measure of the oversubtraction; this should be flat as a function of star magnitude if the background were measured correctly on average.

13.4 Next Steps

The following additional data will need be taken to advance from our current knowledge:

1. g band observations in the EDFS field, when the g filter is put back into ComCam for the upcoming dark time.

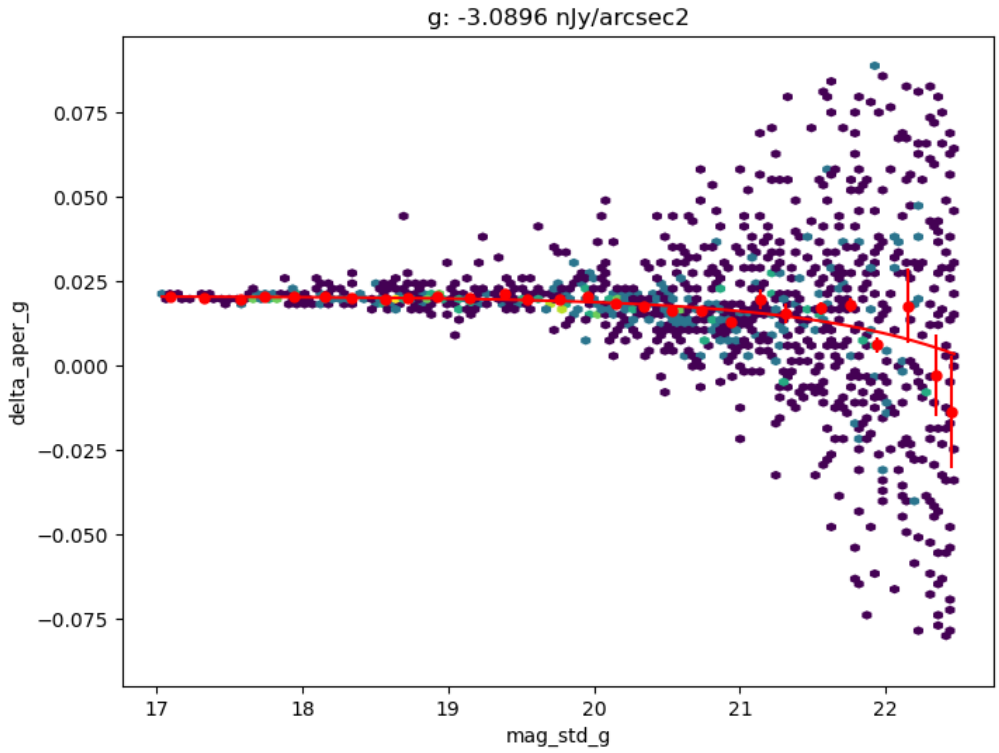

FIGURE 26: Estimate of the background oversubtraction using delta magnitudes from large apertures in the g band. The amount of curvature is a measure of the oversubtraction; this should be flat as a function of star magnitude if the background were measured correctly on average.

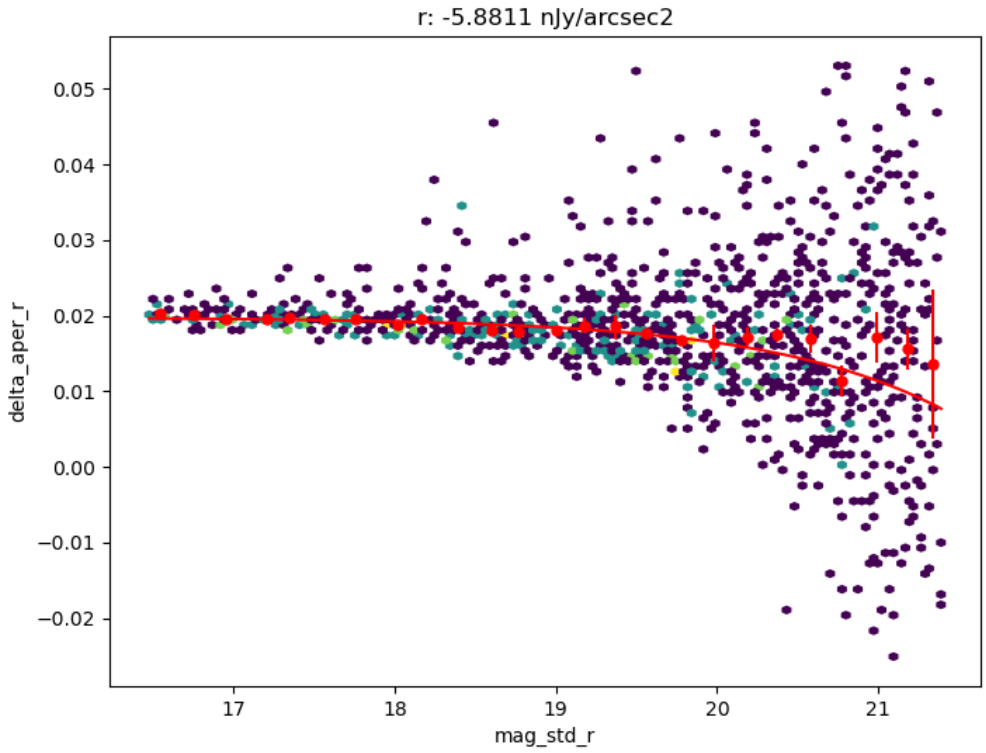

FIGURE 27: Estimate of the background oversubtraction using delta magnitudes from large apertures in the r band. The amount of curvature is a measure of the oversubtraction; this should be flat as a function of star magnitude if the background were measured correctly on average.

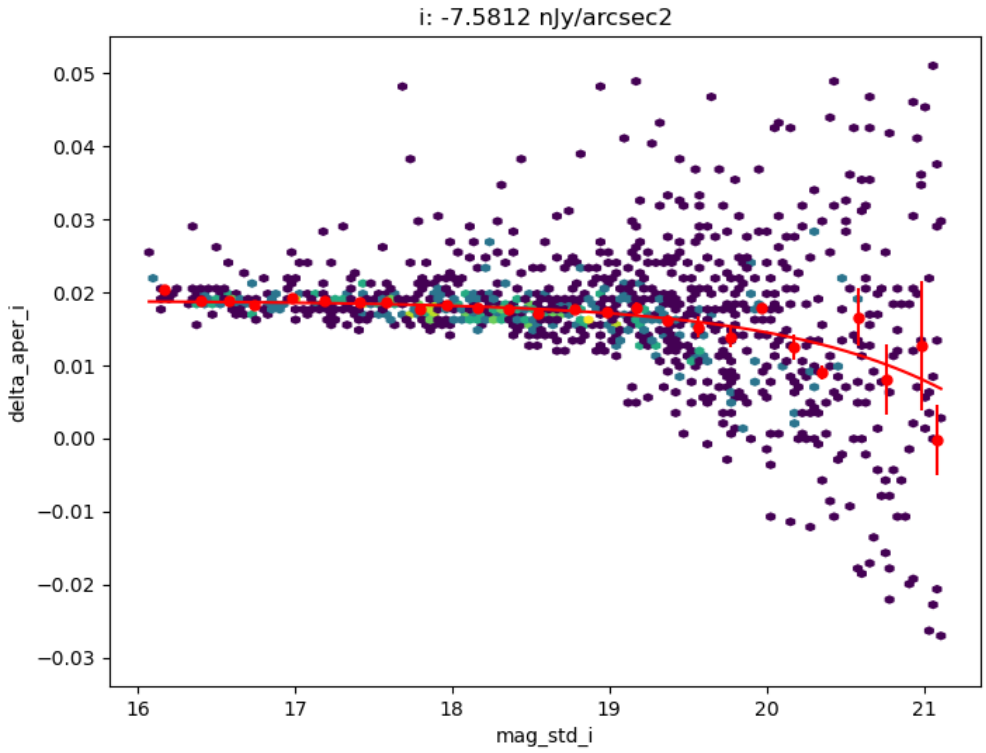

FIGURE 28: Estimate of the background oversubtraction using delta magnitudes from large apertures in the i band. The amount of curvature is a measure of the oversubtraction; this should be flat as a function of star magnitude if the background were measured correctly on average.

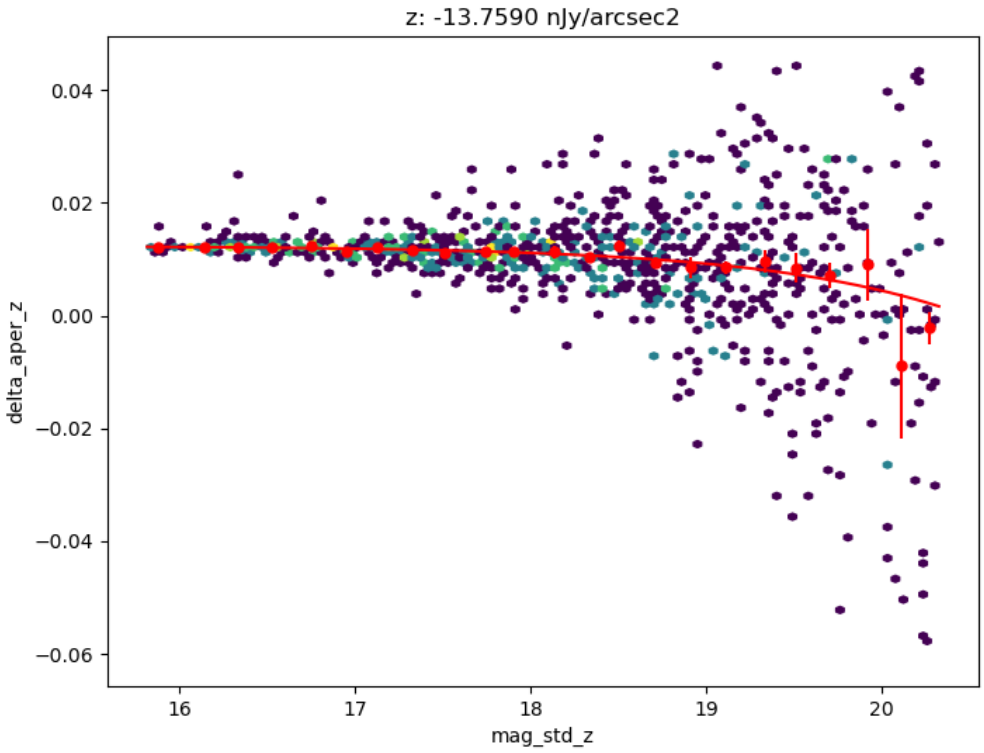

FIGURE 29: Estimate of the background oversubtraction using delta magnitudes from large apertures in the z band. The amount of curvature is a measure of the oversubtraction; this should be flat as a function of star magnitude if the background were measured correctly on average.

2. Dithered observations in as many bands as possible over a field with much larger stellar density for better illumination corrections.
3. More contiguous dithered survey data in (at least) gri.

The particular emphasis on g band in these requests is that by default FGCM will use the $g - i$ color for internal QA, which is a very useful color to split on. There are no facilities in the code for doing quality calibrations on multiple disconnected fields with different band coverage, as this is not the normal case for survey observations. We could run different fields separately with different configs, but this is not preferred. Thus, gri coverage over the fields of interest for DRP processing is the "easiest" path that will yield the best results and be most consistent with the LSST survey.

14 Survey Performance

15 Sample Production

16 Difference Image Analysis: Transience and Variable Objects

17 Difference Image Analysis: Solar System Objects

18 Galaxy Photometry

19 Weak Lensing Shear

20 Crowded Stellar Fields

21 Image Inspection

A References

[SITCOMTN-076], Bechtol, K., on behalf of the Rubin Observatory Project Science Team, S.R., 2024, Information Sharing during Commissioning, URL https://sitcomtn-076.lsst.io/, Vera C. Rubin Observatory Commissioning Technical Note SITCOMTN-076

[LSE-29], Claver, C.F., The LSST Systems Engineering Integrated Project Team, 2017, LSST System Requirements (LSR), URL https://ls.st/LSE-29, Vera C. Rubin Observatory LSE-29

[LSE-30], Claver, C.F., The LSST Systems Engineering Integrated Project Team, 2018, Observatory System Specifications (OSS), URL https://ls.st/LSE-30, Vera C. Rubin Observatory LSE-30

[RTN-011], Guy, L.P., Bechtol, K., Bellm, E., et al., 2024, Rubin Observatory Plans for an Early Science Program, URL https://rtn-011.lsst.io/, Vera C. Rubin Observatory Technical Note RTN-011

B Acronyms

Acronym	Description
2D	Two-dimensional
ADU	Analogue-to-Digital Unit
CBP	Collimated Beam Projector
DES	Dark Energy Survey
DM	Data Management
DR2	Data Release 2
DRP	Data Release Production
EDFS	Euclid Deep Field South
FGCM	Forward Global Calibration Model
HSC	Hyper Suprime-Cam
ISR	Instrument Signal Removal
ITL	Imaging Technology Laboratory (UA)
LATISS	LSST Atmospheric Transmission Imager and Slitless Spectrograph
LSST	Legacy Survey of Space and Time (formerly Large Synoptic Survey Telescope)

MODTRAN	MODerate resolution TRANsmission model
PSF	Point Spread Function
QA	Quality Assurance
QE	quantum efficiency
RTN	Rubin Technical Note
SE	System Engineering
SED	Spectral Energy Distribution
SSP	Solar System Processing